REMARKS

Favorable reconsideration of this application in view of the above amendments and following remarks is respectfully requested.

With respect to the Requirement for Information on page 2 of the outstanding Office Action, Applicants attach herewith, a copy of the published Master's thesis of Andreas Schmid from Reutlingen University entitled Hybrid Solar Cells Device Preparation and Characterization. As discussed on page 3 of the outstanding Office Action, the fee and certification requirements of 37 CFR §1.97 are waived, and therefore are not included herewith.

Claims 1-2, 4 and 6-34 are pending in this application. Claims 25-34 are withdrawn from consideration. By this amendment, Claim 1 is amended; and no claims are added or cancelled herewith. It is respectfully submitted that no new matter is added by this amendment.

In the outstanding Office Action, Claim 1, 2, 4, 6-9 and 19-24 were rejected under 35 U.S.C. § 102(b) as anticipated by Usami; and Claims 9-18 were rejected under 35 U.S.C. § 103(a) as unpatentable over Usami in view of EP 1271,580 to Chone.

It is respectfully submitted that the applied art does not teach or suggest that the porous film includes at least two layers, each layer having a first kind of particle of one average diameter or length and one layer of the at least two layers, having additionally a second kind of particle having a larger average diameter or length, as recited in Claim 1.

Instead, Usami discusses a dye-sensitized nano-crystalline photoelectrochemical cell, which includes a bilayer of TiO_2. The bilayer includes a small particle film and a large particle film. As best shown in Fig. 4 of Usami, the two types of TiO_2 particles used differ in their diameter. Accordingly, Usami does not disclose at least two layers with one type of

particle being present in all of the layers, and additionally having a type of particle with a larger diameter or length in one layer.

The exclusive use of one type of particles in the first layer and the one type of larger particles in the second layer, as discussed by Usami, leads to a strongly reduced absorption strength and, thus, a reduced overall efficiency. In contrast, according to one or more examples of the present invention, the mixture of at least two species of particles in one layer with the one species having the smaller diameter or length is also present in all other layers, allows for altering the scattering strength while keeping the adsorption strength at a substantially constant level. For example, please see Fig. 8 of the present invention.

As acknowledged on page 4 of the outstanding Office Action, Usami discusses the top layers having particles of one average diameter and the two bottom layers have a second kind of particle with a larger average diameter. However, Claim 1 recites in part, that the porous film includes at least two layers, each layer having a first kind of particle of one average diameter or length. Further, one layer of the at least two layers has additionally a second kind of particle having a larger average diameter or length. In Usami, none of the layers individually have two different sized particles. As such, the features of the claimed invention are not taught or suggested by the applied and therefore the applied art cannot provide at least the advantages discussed above.

Similar to Usami, Chone does not discuss a porous film having two layers and in each layer a first kind of particle of one average diameter or length and one layer of the at least two layer includes a second kind of particle having a larger average diameter or length. Instead, Chone discusses a single layer film of metal oxide semiconductor particles, wherein various types of particles are mixed. As discussed throughout the specification of Chone a two-layer system is described but the particles size in both layers are similar. Please see [0031] to [0032] of Chone.

Accordingly, withdrawal of the rejection of the claims under 35 U.S.C. § 102 and §103 is respectfully requested.

Consequently, for the reasons discussed in detail above, no further issues are believed to be outstanding in the present application, and the present application is believed to be in condition for formal allowance. Therefore, a Notice of Allowance is earnestly solicited.

Should the Examiner deem that any further action is necessary to place this application in even better form for allowance, the Examiner is encouraged to contact the undersigned representative at the below-listed telephone number.

Respectfully submitted,

OBLON, SPIVAK, McCLELLAND,
MAIER & NEUSTADT, P.C.

Bradley D. Lytle
Attorney of Record
Registration No. 40,073

Customer Number

22850

Tel: (703) 413-3000
Fax: (703) 413 -2220
(OSMMN 08/07)

Kevin M. McKinley
Registration No. 43,794

I:\ATTY\KMM\PROSECUTION WORK\28\282743\AMEND DUE 1-9-09.DOC

Diplomarbeit

Hybrid Solar Cells
Device Preparation and Characterisation

vorgelegt von
Andreas Schmid

aus
Reutlingen

im Januar 2003

Fachhochschule Reutlingen
-Hochschule für Technik und Wirtschaft-
Fachbereich Angewandte Chemie

Betreuer: Dr. Gabriele Nelles, Sony International (Europe) GmbH

Prof. Dr. Robert Kohler, Fachhochschule Reutlingen
-Hochschule für Technik und Wirtschaft-

Sperrvermerk

Die nachfolgende Diplomarbeit enthält vertrauliche Daten der Firma Sony International (Europe) GmbH. Veröffentlichungen oder Vervielfältigungen – auch nur auszugsweise – sind ohne ausdrückliche Genehmigung der Firma Sony International (Europe) GmbH nicht gestattet. Die Diplomarbeit ist nur den Korrektoren sowie den Mitgliedern des Prüfungsausschusses zugänglich zu machen.

0 Index

0.1 Abbreviations

A	Amount of desorbed dye
AM 1.5	Air mass 1.5
black dye	tris(isothiocyanato)-ruthenium(II)-2,2':6',2''-terpyridine-4,4',4'' tricarboxylic adic
CB	Conduction band
DIPCDI	Diisopropyl carbodiimide
DMF	Dimethylformamide
DMSO	Dimethylsolfoxide
DPTS	4-N,N-dimethylaminopyridinium 4-toluenesulfonate
e^-	Electron
FF	Fill factor
FTO	Fluorine-doped tin oxide
η	Efficiency
$h\nu$	Light quantum
I_{sc}	Short circuit current
IR	Infrared
ITO	indium tin oxide
J_{sc}	Short circuit current-density
N3	Short for used for red dye
θ	Coverage
θ_0	Maximum coverage
θ_e	Remaining coverage of desorbed dye
red dye	cis-bis(isothyiocyanato)bis(2,2'-bipyridyl-4,4'-dicarboxylato-ruthenium(II)
red dye bis-TBA	With tetrabytylammonium hydroxide twice deprotonated form of red dye
S^*	Excited energy state of the dye
S^+	Oxidized state of the dye
S^0	Ground energy state of the dye
TBA	Tetrabutylammonium ion
THF	Tetrahydrofurane
TiO_2	Titanium dioxide
TLC	Thin layer chromatography
UV	Ultraviolet
V_{oc}	Open circuit voltage
VB	Valence band
Vis	Visible light

1 Summary

1.1 Summary

In this work dye sensitised solar cells have been investigated with the overall goal to increase the photovoltaic properties, focusing on the modification of the dye layer. Two strategies have been followed with the goal to increase the amount of injected electrons into the porous layer, i.e. to increase the current density and as a consequence the efficiency. In a first strategy it has been tried to extend the effective absorption range of the adsorbed dye molecules in the visible part of the spectrum. This was done using a mixture of dye molecules showing absorption maxima at different wavelengths. Dyes that have been examined in mixtures were Ru-complexes as red dye bis-TBA, and black dye, as well as different porphyrin dyes with different metal ions.

The dyes used in binary mixtures showed at least a separation of the absorption maximum of 40 to 90 nm.

Adsorption / desorption experiments in combination with UV-Vis-measurements confirmed that the concentration ratio detected at the interface is almost the same as in solution. The coverage of the porous layer with red dye bis-TBA, black dye, and porphyrin Pd was calculated. The coverage for both Ru-complexes is nearly the same, whereas for prophyrin Pd only the half.

Even though we succeeded in extending the effective light absorption range at the dye / titanium dioxide interface, the corresponding solar cells did not reach the performance of our standard solar cell, i.e. containing red dye bis-TBA.

The second strategy is to increase the number of adsorbed dye molecules by adsorbing chemical linked dimers of red dye. Based on the results that dye molecules bridged via silver or cobalt cations show increased efficiencies, but introducing the disadvantage of a further preparation step, a new concept without cations has been developed, in particular a synthesis to get chemically bridged red dye molecules. In a first test system alkyl chains have been introduced via amide or ester linkage. The purification of these new systems was quite difficult; the product could not be separated quantitatively from the side products and therefore could be found in several fractions of the column chromatography. The new dyes have been used to prepare solar cells. The introduction of the alkyl chain changed the features of the dye molecules such that the corresponding solar cells did not reach the performance of the standard solar cell. The precursor

of the bridged dye molecule was realised but the formation of the complex could not be finished within the time frame of this thesis.

1.2 Zusammenfassung

Im Rahmen dieser Diplomarbeit wurden Modifikationen der Farbstoffschicht in farbstoffsensibilisierte Solarzellen untersucht, mit dem Ziel deren photovoltaische Eigenschaften zu verbessern. Hierfür wurden zwei Strategien verfolgt um die Anzahl injizierter Elektronen in die poröse Schicht zu erhöhen, dadurch eine höhere Stromdichte und somit eine höhere Effizienz zu erzielen.

Im Rahmen der ersten Strategie wurde versucht den effektiven Absorptionsbereich der adsorbierten Farbstoffe im sichtbaren Bereich des Spektrums zu erweitern. Dies wurde mit Hilfe von Mischungen aus Farbstoffen gemacht deren Absorptionsmaxima bei verschiedenen Wellenlängen liegen. Untersucht wurden Ruthenium-Komplexe wie Red Dye bis-TBA und Black Dye, sowie diverse Porphyrine mit jeweils verschiedenem Metallion.

Die in zweikomponenten Mischungen verwendeten Farbstoffe wiesen alle eine Verschiebung des Absorptionsmaximums von 40 bis 90 nm auf.

Adsorptions- und Desorptionsexperimente zeigten, in Kombination mit UV-Vis Messungen, dass die Konzentrationsverhältnisse an der Grenzfläche nahezu gleich den Konzentrationsverhältnissen in Lösung sind. Die Bedeckung einer porösen Titandioxid Schicht mit Red Dye bis-TBA, Black Dye und Porphyrin Pd wurde bestimmt. Für beide Ru-Komplexe ist diese nahezu gleich, wohingegen sie für Porphyrin Pd nur halb so groß ist.

Obwohl es möglich war den effektiven Absorptionsbereich an der Farbstoff / Titandioxid Grenzfläche zu erweitern, erreichten die dazugehörigen Solarzellen nicht die Güte von Standardzellen mit Red Dye bis-TBA.

Im Rahmen der zweiten Strategie wurde versucht die Zahl adsorbierter Farbstoffmoleküle zu erhöhen, indem chemisch überbrückte Farbstoffdimere aus Red Dye adsorbiert werden. Gestützt auf Ergebnisse dass Farbstoffe die mit Silber oder Cobalt Ionen verknüpft sind eine erhöhte Effizienz ergeben, jedoch den Nachteil mit sich bringen einen zusätzlichen Schritt im Herstellungsprozess zu benötigen, wurde ein neues Konzept entwickelt für welches keine Kationen notwendig sind: Die Synthese eine chemisch überbrückten Red Dye Moleküls. In einem ersten Testsystem wurden Alkylketten über Amid- und Esterbindungen an ein Farbstoffmolekül geknüpft. Die Reinigung dieser neuen Systeme gestaltete sich jedoch ziemlich

schwierig, da das Produkt nicht vollständig von Nebenprodukten getrennt werden konnte. Die neuen Farbstoffe wurden in Solarzellen getestet. Vermutlich änderte die Anknüpfung der Alkylketten die Eigenschaften der Farbstoffmoleküle, so dass die zugehörigen Solarzellen nicht die Güte von Standard Solarzellen erreichten. Die Vorstufen des überbrückten Moleküls wurden verwirklicht, jedoch war es im zeitlichen Rahmen dieser Arbeit nicht mehr möglich den kompletten Komplex herzustellen.

2 Introduction and aim of the thesis

With the beginning of observations by Benjamin Franklin and inventions by Volta, Ampere, Watt and Edison, electricity and electrical energy has been and still is steadily becoming important and used as energy for thousands of processes. Nowadays electricity is almost ubiquitous in daily life, mainly produced in coal-fired or nuclear power plants. Recently the demand of sustainable and environmental friendly forms of energy production becomes more and more important. Besides wind and water power, solar power is an important energy source.

Since Sony develops various portable electronic devices it would be beneficial to introduce an independent power supply like solar cells. The solar cells commonly used are made of silicon. However, during the production process a lot of energy is needed, and the costs of such solar cells are still quite high. In contrast, a new type of hybrid solar cells developed in the group of Prof. Grätzel offers a significant reduction of the costs due to their simple construction, by still reaching almost the same efficiency as amorphous silicon solar cells. The key idea is to have a huge surface of a semiconductor, which is sensitised by adsorbed dye molecules. The dye absorbs light and injects electrons into the semiconductive layer, which creates electron-hole pairs.

The aim of the present work is to modify the dye layer in such a dye-sensitised solar cell with the final goal of improving the efficiency by increasing light absorption. In particular, two strategies will be followed to enlarge the number of injected electrons. The first concept is to extend the effective absorption range of the adsorbed dye molecules in the visible part of the spectrum, using a binary dye mixture. The second concept to be followed is to increase the number of adsorbed dye molecules by adsorbing chemically linked dimers of dye molecules. The influence of these two concepts will be tested in real solar cells.

3 Theoretical Background

3.1 Dye-sensitised solar cells

Solar energy is a steadily growing energy-technology today, and solar cells have found markets in a wide variety of applications. The conversion of solar light into electric power requires the generation of both negative and positive charges, charge separation, as well as a driving force that can push these charges through an external electric circuit.

Until now, photovoltaics, devices that convert sunlight to electrical power, have been dominated by solid-state junction devices, often made of silicon. A new generation of photovoltaic cells are the dye-sensitised solar cells.[i] That provide a technically and economically credible alternative concept. Historically the dye-sensitisation dates back to the 19th century, when photography was invented[ii]. The use of dye-sensitisation in photovoltaics remained however rather unsuccessful until a breakthrough in the early 1990's in the laboratories of professor Grätzel in Switzerland. By the successful combination of nanoporous electrodes and efficient charge injection dyes, Grätzel and his co-workers developed a solar cell with energy conversion efficiency exceeding 7 % in 1991.

In contrast to the conventional systems light absorption and charge carrier transport is here separated. Light is absorbed by a sensitiser, a dye, which is anchored to the surface of a wide band gap semiconductor, titanium dioxide (TiO_2). Charge separation takes place at the interface via photo-induced electron injection from the dye into the conduction band of the titanium dioxide. Carriers are transported in the conduction band of the semiconductor to the charge collector. The use of transition metal complexes as dyes, having a broad absorption band in conjunction with oxide films of nanocrystalline titanium dioxide, permits the harvesting of a large fraction of sunlight. Near-quantitative conversion of incident photons into electric current is achieved over a large spectral range extending over the whole visible region. [iii]

3.1.1 Design

The cell is constructed in a sandwich configuration. The working electrode is nanoporous TiO_2 placed on a conducting glass slide support, on which a thin layer of TiO_2 is applied.

This electrode is separated with a 6-μm thick spacer foil from the counter electrode. Between the two electrodes there is the electrolyte with a redox-couple such as I^-/I_3^-. The dye is chemically adsorbed at the TiO_2 surface. The counter electrode is also made of conducting glass with a thin layer of platinum sputtered onto it to reduce overpotentials. Illumination occurs through the working electrode.
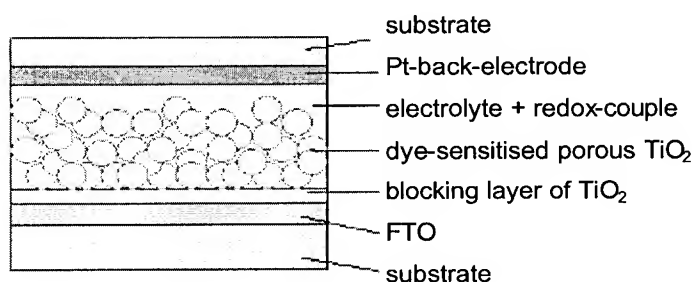

substrate
Pt-back-electrode
electrolyte + redox-couple
dye-sensitised porous TiO_2
blocking layer of TiO_2
FTO
substrate

Figure 3-1. Schematic structure of a dye-sensitised solar cell

3.1.2 The different layers

- Substrates: the electrodes are transparent conducting oxide glass substrates. The conducting coating works as a current collector, and is usually fluorine-doped tin oxide (SnO_2:F or FTO). In contrast to indium tin oxide (In_2O_3:Sn or ITO) the oxidation state of FTO is stable at temperatures around 450-500 °C that are reached in the preparation process of the nanoporous TiO_2 films. For the working electrode the transparency is important since illumination occurs through this electrode. To be used as counter electrode, the substrate is coated with platinum to reduce overpotentials.

- Blocking layer: the working electrode is coated with a small layer of titanium dioxide. This layer prevents the recombination of electrons, and guides the electrons in the wanted direction through the external circuit.

- Dye-sensitised porous titanium dioxide: oxide semiconductors are preferential in photo electrochemistry because of their exceptional stability against photo corrosion on optical excitation in the band gap[iv]. Furthermore, the large band gap (>3 eV) of the oxide semiconductors is needed in dye-sensitised solar cells to enable a transparency for a large

part of the solar spectrum. Two morphologies of TiO_2 are important, anatase and rutile. Anatase appears as pyramid-like crystals and is stable at low temperatures, whereas needle-like rutile crystals are dominantly formed at high temperature processes over 500 °C. The band-gaps of the crystalline forms are 3.2 eV for anatase (the absorption edge at 388 nm) and 3.0 eV for rutile (the absorption edge at 413 nm). Anatase has an advantage over rutile as the short-circuit current is higher than of rutile-based solar cells[v], related to a higher amount of adsorbed dye, owing to a higher surface area per unit volume of the anatase porous layer compared with that of a rutile porous layer. Also the electron transport is reported to be slower in the rutile layer than in the anatase layer due to differences in the extent of interparticle connectivity associated with the particle packing density[v]. The pastes contain nanoparticles of TiO_2. To get a viscous paste needed for the preparation several organic substances are added. For the paste K65 the organic compounds are 65 percent by weight, for the K40 paste 40 percent by weight.

- The electrolyte allows the charge transport inside the cell. The containing redox couple is I^-/I_3^-.

3.1.3 Working Principle

The working cycle of a dye-sensitised solar cell is depicted in Figure 3-2, showing schematically the relative energy levels of the working cell.
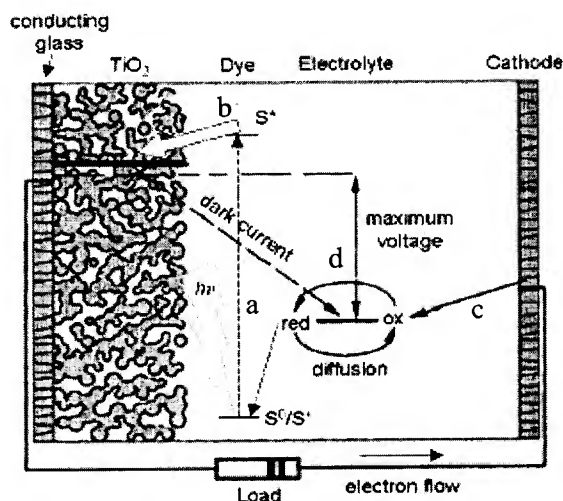

Figure 3-2. Working principle of dye-sensitised solar cells

The incoming photon is absorbed by a dye molecule, which is adsorbed at the surface of the titanium dioxide particle. Consequently, the dye will be promoted into its excited state S^* (a) from where it is now energetically able to inject an electron into the TiO_2 conduction band, leaving the dye in an oxidised state S^+ (b). The injection takes place if the lifetime of this excited state is long enough, the energy level of the TiO_2 conduction band is lower than that of the excited state S^*, and if the injection occurs faster than the recombination. The recombination of the dye by the redox couple has to be faster than the recombination from the $TiO2$ side by an injected electron. The electron can penetrate the nanoporous TiO_2 layer to the conducting glass substrate and finally through an external circuit load to the counter electrode. At the counter electrode /electrolyte interface the electron is caught by a redox couple, where iodine is reduced to iodide (c). The cycle is closed by oxidation of iodide to iodine (d). This process is diffusion controlled. The operation cycle can be summarised in chemical reaction terminology as[vi]:

$$S + h\nu \rightarrow S^* \qquad \text{(a)}$$

$$S^* \rightarrow S^+ + e^-(TiO_2) \qquad \text{(b)}$$

$$I_3^- + 2e^-(Pt) \rightarrow 3I^- \qquad \text{(c/2)}$$

$$2S^+ + 3I^- \rightarrow 2S + I_3^- \qquad \text{(d)}$$

$$S^* \rightarrow S \qquad \text{(a1)}$$

$$S^+ + e^-(TiO_2) \rightarrow S \qquad \text{(1)}$$
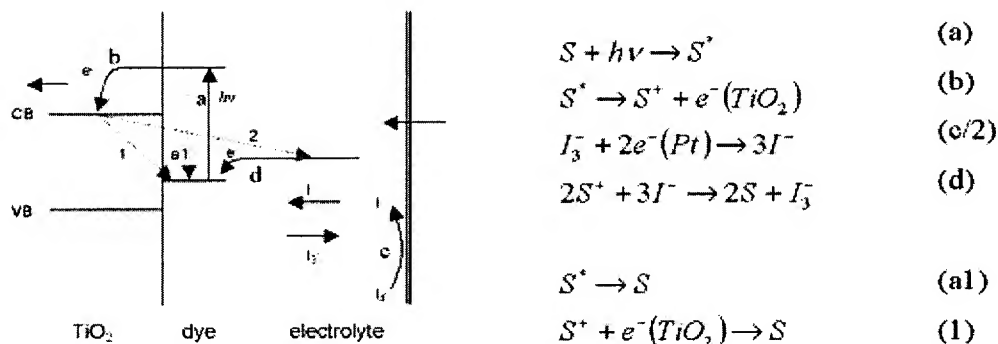
Figure 3-3. Reaction steps in a solar cell

Several reactions need to be considered which may lower the performance of dye-sensitised solar cells. These reactions are[vii]:

- Excited state decay (a1): the electron injection (b) or the regeneration (d) of S^+ by I^- needs to be faster than the decay.

- Electron recombination with oxidised dye (1): an electron from the TiO_2 conduction band recombines with the oxidised dye S^+ at the TiO_2 electrode surface.

- Electron recombination with redox couple (2): an electron from the TiO_2 conduction band recombines with the oxidised form I_3^- of the redox couple.

- Bleaching of dye: if the oxidised form of the dye S^+ is not stable at the time scale over which it is reduced back to its ground state S^0, it will decompose and hence, the solar cell will bleach.

3.2 The Dye

3.2.1 Fundamentals

The two desirable properties of the dye are absorption of visible light and electron injection to the titanium dioxide.

To achieve a high energy conversion efficiency, the properties of the dye molecule, as attached to the semiconductor particle surface, are essential.

The dye should absorb light at wavelengths up to 900 nm. To minimise energy losses and maximise the photo voltage, the excited state of the adsorbed dye molecule should only be slightly above the conduction band edge of the TiO_2, but yet above enough to present an energetic driving force for the electron injection process. For the same reason, the ground state of the molecule should only be slightly below the chemical potential of the redox-couple I^-/I_3^- in the electrolyte.

The process of electron injection from the excited state to the conduction band of the semiconductor should be fast enough to outrun competing unwanted relaxation and reaction pathways. To ensure electronic contact between the dye and the titanium dioxide, as well as a stable adhesion at the interface, to prevent dissolving of the dye in the electrolyte, chemical attachment of the dye to the semiconductor via functional groups is necessary. This is done in a self-assembly process. The adsorbed dye molecules should be stable enough in the working environment.
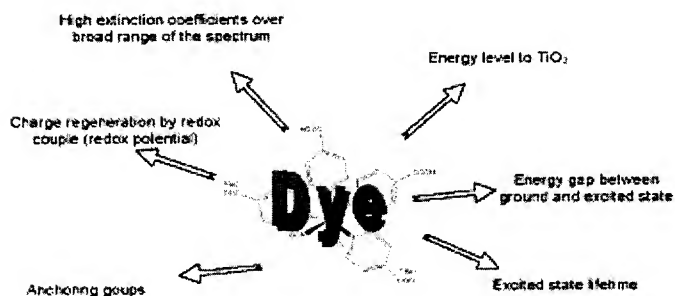

Figure 3-4. Major requirements for the dye in dye-sensitised solar cells

3.2.2 State of the art

Most sensitisers currently used in solar cell applications are ruthenium polypyridyl complexes. The development of sensitisers over the past two decades is summarised in the Figure 3-4. Over this period, more than 900 sensitisers have been specifically synthesised and tested for solar cell applications[viii], but only those few displayed below gave satisfactory performances. Most of these sensitisers are ruthenium complexes; some are osmium[ix] complexes, pure organic dyes[x] or other compounds. So far, it is not understood, why only a very small fraction of dyes perform well as photosensitisers, whilst the majority of dyes, with very similar chemical and physical properties, do not.
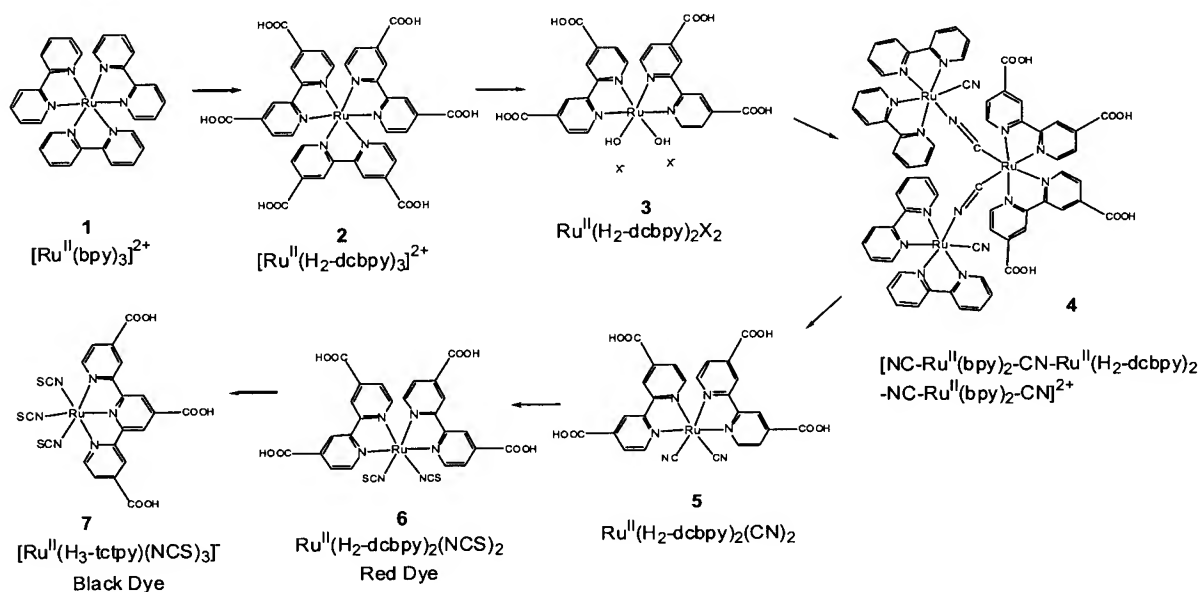

Figure 3-5. Historic development of sensitisers for solar cells.

Ruthenium polypyridyl complexes are the most performant sensitisers known so far, with a unique combination of efficient charge injection, broad visible spectrum, and long-term stability. Cells made of the following dyes show already good results:

cis-bis(isothiocyanato)bis(2,2'-bipyridyl-4,4'-dicarboxylato)-ruthenium(II) (6), which is also called N3 or 'red dye' and

cis-bis(isothiocyanato)bis(2,2'-bipyridyl-4,4'-dicarboxylato)-ruthenium(II)bis-tetrabutylammonium , the twice deprotonated form, and

tris(isothiocyanato)-ruthenium(II)-2,2':6',2''-terpyridine-4,4',4''- tricarboxylic acid (7), also called 'black dye', due to its dark colour in the solid state. Despite the wider absorption spectrum, the cells made with black dye do not show as good results as the one made of red dye. Some of the dyes investigated within the last years are already commercially available.

3.3 Characterisation

In order to determine photovoltaic characteristics of solar cells, current-voltage curves (I-V-curves) are measured. A voltage is applied to the cell and linearly changed (swept) with time from the starting to the end potential. The rate of voltage change with time is called the scan rate. From the resulting I-V-curve the solar cell performance can be determined as explained later.

According to a standard, the cells are measured in the dark, and under illumination with white light with an intensity of 100 $mW\cdot cm^{-2}$ (measured at 530 nm). Furthermore, the measurements are done with reduced light intensities of 80, 50, 25 and 10 $mW\cdot cm^{-2}$.
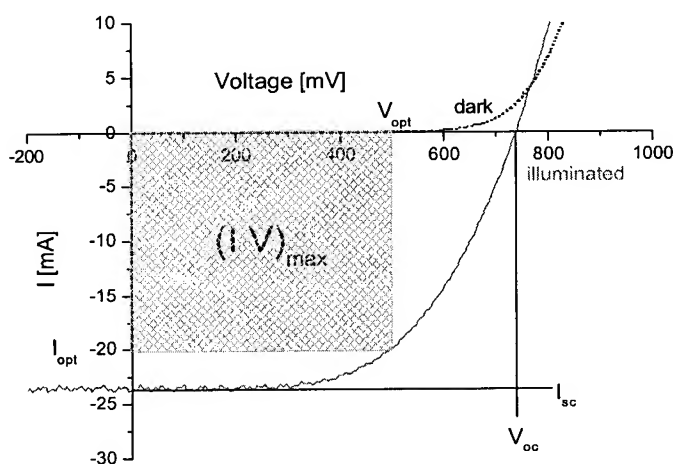
Figure 3-6. Charactersistic I-V-Curve of a solar cell. V_{oc} and I_{sc} are the open circuit voltage and the short circuit current. V_{opt} and I_{opt} are the voltage and current at the optimal operating point.

3.3.1 Short circuit current, I_{sc}

I_{sc} is the current obtained when the solar cell is short-circuited, i.e. if there is no potential across the cell. The short circuit current is equal to the absolute number of photons converted to hole-

electron pairs. If the short circuit current is referred to the area of the cell it is called the short circuit current density J_{sc}.

3.3.2 Open circuit voltage, V_{oc}

Under open circuit conditions no current can flow and the voltage is at its maximum, this is called the open circuit voltage V_{oc}.

3.3.3 Fill Factor, FF

Optimal power output requires a suitable resistor, which corresponds to the ratio V_{opt}/I_{opt}. V_{opt} and I_{opt} are the voltage and current at the optimum operating point and $V_{opt} \cdot I_{opt} = P_{opt}$ is the maximum achievable power output $(IV)_{max}$. The ratio of peak output $(IV)_{max}$ to $V_{oc}I_{sc}$ is called the Fill Factor (FF) of a solar cell and is an important quality criterion.

$$FF = \frac{(I \cdot V)_{max}}{V_{oc} \cdot I_{sc}}$$

Equation 3-1. Determination of the Fill Factor, FF.

The name Fill Factor is derived from its graphical representation. It indicates how much area underneath the I-V-curve is filled by the rectangle described by $(IV)_{max}$ (shaded area) in relation to the rectangle $V_{oc}I_{sc}$.

3.3.4 Efficiency, η

The energy conversion efficiency of a solar cell is defined as the ratio of the photovoltaic generated electric output and the energy of the incident irradiant solar light.

$$\eta = \frac{P_{out}}{P_{in}} = \frac{(I \cdot V)_{max}}{L \cdot A} = \frac{FF \cdot I_{sc} \cdot V_{oc}}{L \cdot A}$$

Equation 3-2. Determination of the power conversion efficiency. P_{out} is the output power, P_{in} the input power, L is the intensity of the light, and A the active area of the cell.

The solar cell performance depends on the temperature of the cell, and what is even more important, on the quality of the illumination, i.e. the total light intensity and the spectral distribution of the intensity. For this reason, a standard measurement condition has been developed to facilitate comparable testing of the solar cells between different laboratories. In the standard condition used for testing of terrestrial solar cells the light intensity is 1000 W/m^2, the

spectral distribution of the light source is that of AM-1.5 global standard solar spectrum (Figure 3-7), and the temperature of the cell is 25°C.
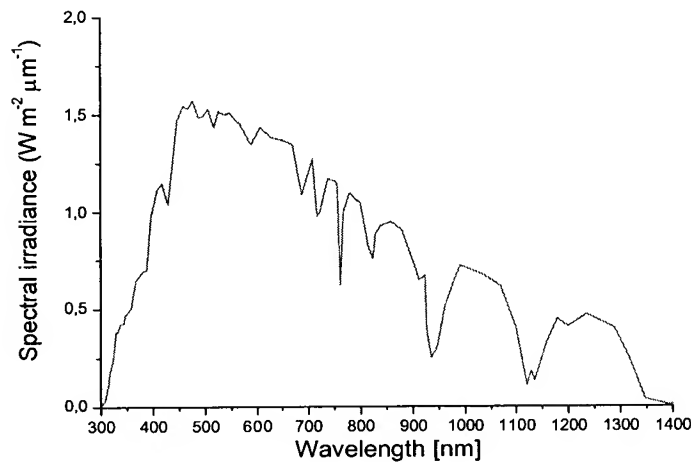

Figure 3-7.The standard AM-1.5 global solar spectrum.

3.3.5 Conditions for the Light source

Specific solar radiation conditions are defined by the Air Mass (AM) value. The spectral distribution and total flux of radiation just outside the Earth's atmosphere, similar to the radiation of a black body of 5800K, has been defined as AM-0. In passing through the atmosphere the radiation becomes attenuated by complex and varying extinction processes. At the equator at sea level at noon when the incidence of sunlight is vertical (90°, sun in zenith) and the light travels the shortest distance through the atmosphere and air ("air-mass") to the surface, the spectral solar radiance and flux (1.07kWm²) is defined as AM-1. However, if the angle of light incidence is smaller than 90°, the light has to travel through more air mass than under AM-1 conditions. The relative path length through the atmosphere by the shortest geometrical path is given by:
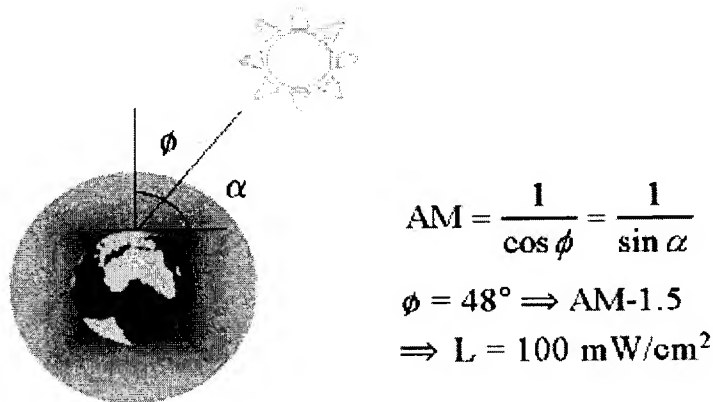
$$AM = \frac{1}{\cos \phi} = \frac{1}{\sin \alpha}$$

$$\phi = 48° \Rightarrow AM\text{-}1.5$$

$$\Rightarrow L = 100 \text{ mW/cm}^2$$

Figure 3-8. Standard light intensity. Angle of light incidence measured to the horizon (α), to the normal (ϕ).

The relationship described is only valid for a planar atmosphere, but only introduces an error of less than 1% from the curved atmosphere of the Earth, if $\alpha > 20°$.

The so-called AM-1.5 conditions are achieved when the sun is at an angle of 48.1° above the horizon and results in a solar flux of 963W m^{-2}. This angle of incidence is commonly encountered in western countries and hence AM-1.5 is taken as a standard condition for solar cell testing and referencing. In the last few years, the AM-1.5 spectrum has been standardised. For convenience, the flux of the standardised AM-1.5 spectrum has been corrected to 1000Wm^{-2} (100 mW cm^{-2}). However, despite availability of standards, great care has to be taken when results reported in the literature are compared. For example, often AM-1.5 conditions are reported, but this may only mean that a radiance of 1000 Wm^{-2} has been used, with the proper spectral distribution being neglected.

4 Experimental Part

The objective of the present work is to modify the dye in dye-sensitised solar cells with the final goal of improving the efficiency. As already mentioned a suitable dye molecule should be able to inject electrons into the titanium dioxide after light absorption. To increase the efficiency of a dye-sensitised solar cell, by means of the dye, the light absorption has to be improved. This goal can be achieved both by extending the effective absorption range of the adsorbed dye molecules in the visible part of the spectrum, or by increasing the concentration of adsorbed dye at the interface of the porous TiO_2 layer.

4.1 Extending the effective absorption range of adsorbed dye molecles

The idea behind the work described in this paragraph is to increase the light absorption by extending the effective absorption range of the adsorbed dye molecules in the visible part of the spectrum, especially to higher wavelengths.

This shall be realised using mixtures of different dye molecules showing different absorption spectra. The absorption maximum of those dyes should be separated from each other, and the spectra should be additive.

4.1.1 Mixtures of Ru-Complexes

The two Ru-complexes cis-bis(isothiocyanato)bis(2,2'-bipyridyl-4,4'-dicarboxylato)-ruthenium(II) bis-tetrabutylammonium (red dye bis-TBA) and tris(isothiocyanato)- (2,2':6',2"-terpyridine-4,4',4"-tricarboxylic acid)-ruthenium(II) (black dye) are known from the literature to give reasonable results when applied to dye-sensitised solar cells. These two commercially available sensitisers are investigated pure and in mixtures. Their UV-Vis-spectra in ethanol are recorded and correlated with their performance in solar cells.
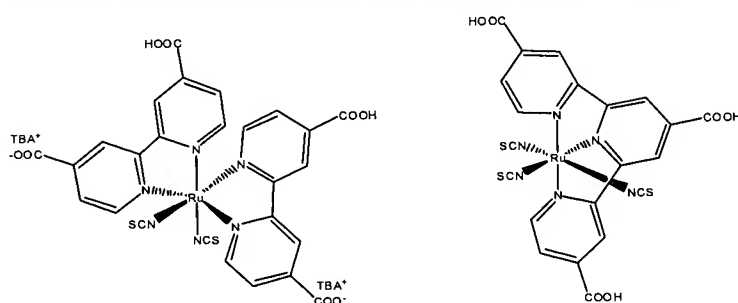

Figure 4-1. Chemical structure of red dye bis-TBA (left), and black dye (right).

Results from earlier experiments show that red dye bis-TBA gives so far the best results, however, its absorption spectrum shows a maximum at 530 nm, whereas the absorption maximum of black dye is shifted to higher wavelength, at 615 nm.

In this experiment mixtures of these two dyes are prepared to check whether it is possible to get an extended absorption spectrum, which is the sum of the single spectra, and if the absorption range can be extendend if this has a positive impact on the solar cell performance.

Solutions of these two dyes are prepared with a concentration of $3.0 \cdot 10^{-4}$ mol·L^{-1}, using ethanol as solvent, as well as mixed solutions with ratios red dye bis-TBA : black dye 3:1, 1:1, and 1:3. Nanoporous layers of TiO$_2$ are prepared (see paragraph 4.4.3), and they are immersed in the dye solutions. The standard concentration for the dye adsorption to a nanoporous layer of TiO$_2$ is $3.0 \cdot 10^{-4}$ mol·L^{-1}, whenever spectra are measured a diluted solution is used because at the standard concentration, the absorbance values are outside the measurement range of the spectrometer.
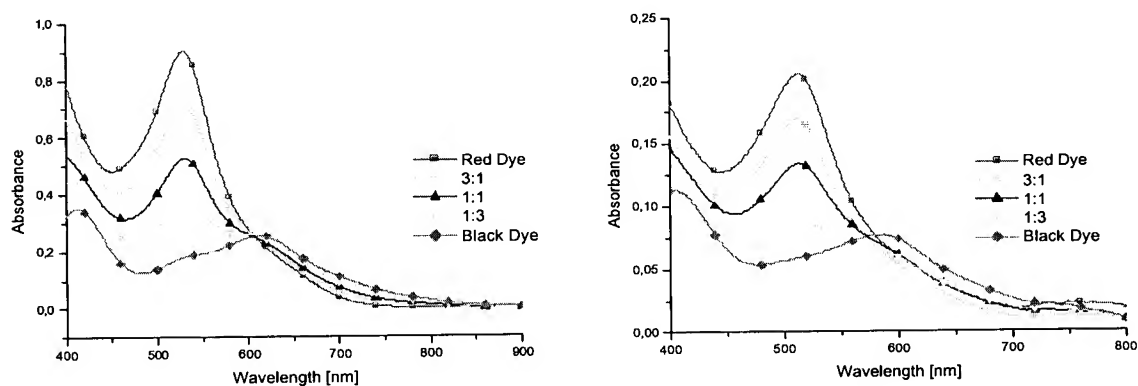
Figure 4-2. Spectra of red dye bis-TBA, and black dye, as well as mixtures of both. Measured in solution in ethanol at a total concentration of $7.0 \cdot 10^{-5}$ mol·L^{-1}(left). Measured after performing desorption experiment in aquesous solution (right).

After 16 hours the substrates are removed, rinsed with ethanol and dried with nitrogen. With the coloured substrates desorption experiments are performed. With 5 mL of sodium hydroxide solution (c=1.0 mol·L^{-1}) the dye is washed into a 10 mL volumetric flask and filled with distilled water. From those solutions UV-Vis-spectra are collected, they can be seen in Figure 4-2. The absorption spectra of the fresh dye solutions and the desorbed dye solutions are comparable with respect to the peak ratios. As a result it seems that the ratio of the two dyes adsorbed at the titanium dioxide interface is the same as was in the adsorption solution.

A quantitative description of the determination of the concentrations will be given in chapter 4.1.4 that confirms this observation.

The next step is the preparation of photovoltaic devices, using the above mentioned dye mixtures.

After the blocking layer is applied on FTO substrates, the porous layer of TiO_2 is printed using a paste K65 and net with mesh size 30. The sintered films are stored for 16 h in the dye solution. Then the substrates are cut in the middle and the electrolyte is added. After another night the cells are measured. The current-voltage curves and the table containing the corresponding results are shown in Figure 4-3 and Table 4-1.
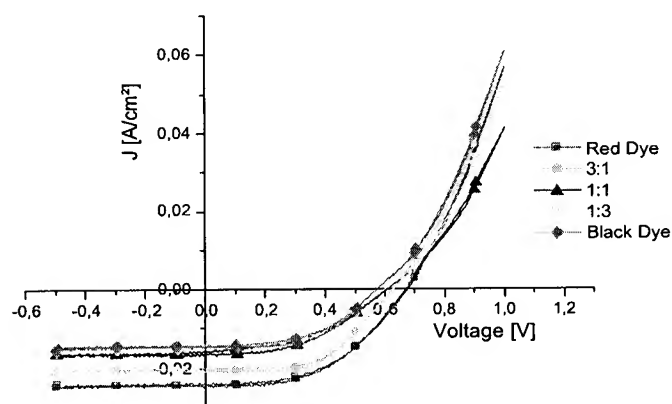

Figure 4-3. I-V-curves of cells with different dyes, and their mixtures. Measured at 100 mW/cm² light intensity.

Table 4-1. Results of cells made of red dye bis-TBA and black dye mixtures, illuminated with 100 mW/cm².

Mixture	J_{sc} [mA/cm²]	V_{oc} [mV]	FF [%]	Efficiency [%]
red dye bis-TBA	24.1	670	50	8.0
3:1	20.8	625	55	7.1
1:1	16.5	605	55	4.6
1:3	15.1	600	46	4.2
black dye	14.8	575	54	4.6

Red dye bis-TBA gives good results (8 % efficiency) when it is used pure. The cells containing an increasing amount of black dye, give worse results. With increased black dye concentration in

the mixture the current density considerably decreases and this is reflected in the efficiency. This trend can be verified with Figure 4-4, where the short circuit current density and the efficiency are plotted against the concentration ratio. The short circuit current density decreases linearly with increasing black dye concentration. The same trend can also be seen for the efficiency but as the fill factor changes irregularly the decrease is not that linear.
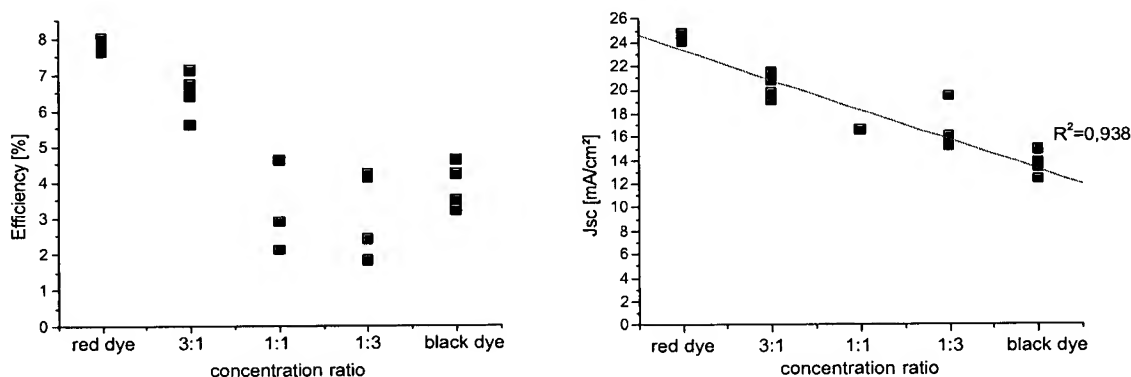

Figure 4-4. Plot of efficiency (left) and short circuit current density (right) versus the concentration ratio. The linear decrease of the current density with increasing black dye concentration can be seen.

The increasing amount of black dye cannot compensate the decreasing absorption that would result from red dye bis-TBA, since the performance of black dye alone is not sufficient. The absorption maximum of black dye is at the edge of the absorption maximum of red dye bis-TBA, and also the intensities at this wavelength are almost the same.

A different group of dyes, porphyrines, has been tested. Here the absorption maximum in the spectra are more shifted.

4.1.2 Porphyrin dyes

Porphyrines are widely known and investigated materials because of their remarkable photophysical properties such as high polarisability and high nonlinear optical behaviour, which are also of current interest for their potential use as molecular wire[xi]. A lot of different modifications are commercially available. Due to the fact that porphyrines with same structure but different central ions show different absorption spectra, it might be possible to get a mixture with a broad absorption spectrum that can be used in solar cells.

Several porphyrins having the same structure but with different metal-ions are tested (Figure 4-5). The free carboxylic acid groups allow the chemical adsorption to the titanium dioxide. Ethanolic porphyrin solutions ($c=3.0 \cdot 10^{-4}$ mol·L^{-1}) are prepared for all the porphyrines described in Figure 4-5.

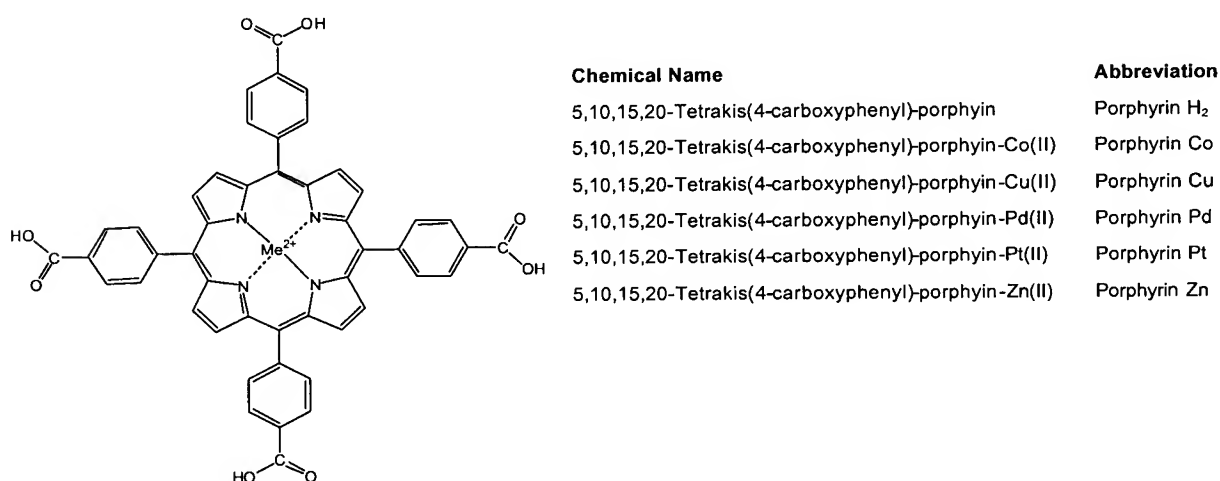| Chemical Name	Abbreviation
5,10,15,20-Tetrakis(4-carboxyphenyl)-porphyin	Porphyrin H$_2$
5,10,15,20-Tetrakis(4-carboxyphenyl)-porphyin-Co(II)	Porphyrin Co
5,10,15,20-Tetrakis(4-carboxyphenyl)-porphyin-Cu(II)	Porphyrin Cu
5,10,15,20-Tetrakis(4-carboxyphenyl)-porphyin-Pd(II)	Porphyrin Pd
5,10,15,20-Tetrakis(4-carboxyphenyl)-porphyin-Pt(II)	Porphyrin Pt
5,10,15,20-Tetrakis(4-carboxyphenyl)-porphyin-Zn(II)	Porphyrin Zn

Figure 4-5. Chemical structure of porphyrines used

The absorption spectra are reported in Figure 4-6.
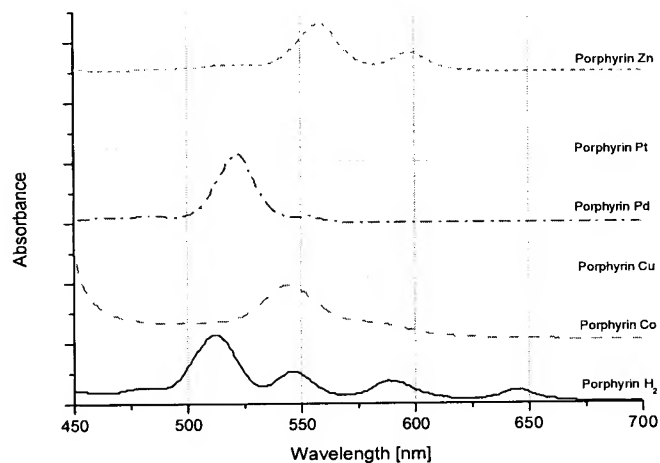
Table 4-2. Absorption maxima of porphyrins in ethanol

Dye	Absorption maximum [nm]
Porphyrin Zn	558
Porphyrin Pt	509
Porphyrin Pd	523
Porphyrin Cu	538
Porphyrin Co	544
Porphyrin H$_2$	512

Figure 4-6. Spectra of the porphyrines, in ethanol; $c=1.2 \cdot 10^{-4}$ mol·L^{-1}.

As these dyes have not yet been used in solar cells, solar cells have been prepared using these different dyes to get first information about the performance of the pure dyes.

The standard electrolyte cannot be used in this case, because the porphyrin dyes are dissolved in THF. A series of experiments has been done in order to find out a suitable solvent. Acetonitril has been found to be the best choice.

The characteristic values of the cells are summarised in Table 4-3.

Table 4-3. Results for solar cells made of the different porphyrin dyes.

Dye	J_{sc} [mA/cm²]	V_{oc} [mV]	FF [%]	Efficiency [%]
porphyrin H₂	1.35	360	59	0.29
porphyrin Co	0.01	310	68	2.50E-03
porphyrin Cu	0.83	375	60	0.19
porphyrin Pd	7.71	530	70	2.86
porphyrin Pt	1.22	420	75	0.38
porphyrin Zn	4.06	495	73	1.47

Only cells with porphyrin Pd and porphyrin Zn give efficiencies over 1 %, though the value for porphyrin Pd of 2.9 % is far behind the values achieved with red dye bis-TBA.

The reason for the different performance are probably due to the HOMO/LUMO values, that only for porphyrin Pd and porphyrin Zn are suitable towards TiO_2-injection or the redox-couple of the electrolyte for the regeneration of the dye. Attempts to determine the redox-potential with cyclic voltammetry did not provide conclusive results, and due to a lack of time this could not be repeated in the frame of this work.

From the results mentioned above only porphyrin Pd and porphyrin Zn show reasonably acceptable performance, therefore the focus was on these two dye molecules. These two are investigated in more detail and also their behavior in mixtures is tested.

Mixtures of porphyrin Pd and porphyrin Zn have been investigated. The absorption at the maximum of porphyrin Zn is about half of the maximum absorption of porphyrin Pd, so a mixture of Pd:Zn 1:2 seems to be the most promising, but also ratios of 1:1 and 2:1 are prepared and measured. Solutions of the mixtures in ethanol are prepared and films are coloured over night. The UV-Vis-spectra are reported in Figure 4-7.
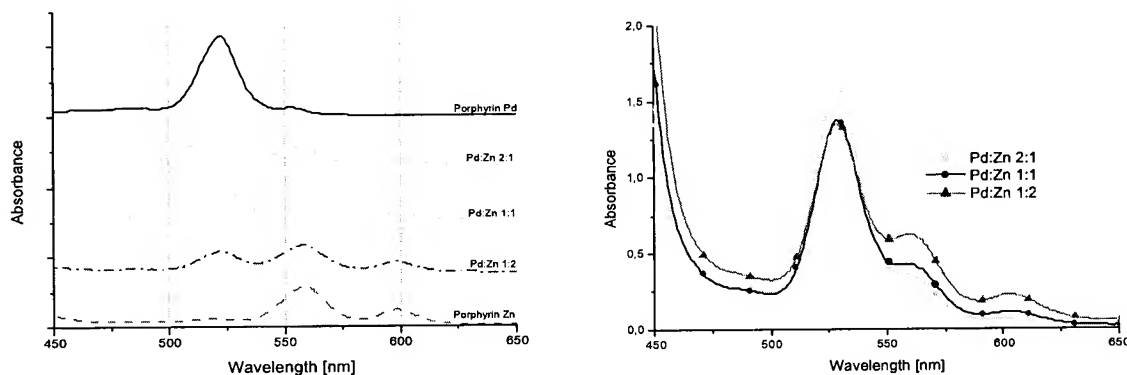
Figure 4-7. Spectra of the solutions of porphyrin Pd and Zn and mixtures (left); spectra of the coloured porous layers of Ti O_2 with mixtures (right).

From the spectra in solution it can be seen that the suggested mixture porphyrin Pd:Zn 1:2 shows two major maxima with nearly same intensity. Differently, porous layers of TiO_2 coloured with the mixtures give quite a different result. The absorption peak resulting from porphyrin Pd at 523 nm is more intense than the porphyrin Zn peak at 558 nm, showing that probably more porphyrin Pd has been adsorbed at the TiO_2 surface.

The characteristic values of the cells are reported in Table 4-4. The performance of the solar cell with porphyrin Pd could be improved to an efficiency of 4.0 % and a current density of 10.7 mA/cm². The solar cells based on mixtures and on pure porphyrin Zn show efficiencies between 1.54 and 1.92 %.

Table 4-4. Results for cells with mixtures of porphyrin Pd and porphyrin Zn under 100 mW/cm² illumination (measured at 530 nm).

Modification	J_{sc} [mA/cm²]	V_{oc} [mV]	FF [%]	Efficiency [%]
Porphyrin Pd	10.70	555	68	4.03
Pd:Zn 2:1	5.58	485	71	1.92
Pd:Zn 1:1	4.46	480	72	1.54
Pd:Zn 1:2	4.96	490	69	1.68
Porphyrin Zn	4.62	490	71	1.62

For the dyes used in this experiment the spectra were well separated and the mixture spectrum of the 1:2 mixture showed an extended absorption range. But the electron injection capability of

these two dyes was too different, more distinct for porphyrin Pd and less for porphyrin Zn. Therefore the increasing porphyrin Zn ratio decreases the short circuit current density.

4.1.3   Mixture of a porphyrin dye and Ru-complex

In the two previous experiments the use of mixtures did not result in an increased performance of solar cells made of these mixtures. In the first experiment with the Ru dye mixture the absorption spectra were not separated well, where in the second experiment with the porphyrin Pd / Zn mixture the spectra were appropriate but electron injection capability was too different.

Therefore in this mixture experiment black dye and porphyrin Pd are used. They show well-separated absorption spectra and a comparable performance in solar cells, efficiency of 4 %, when use pure. A mixture of black dye and porphyrin Pd in same ratio is tested upon its results in a solar cell. A 1:1 mixture solution of black dye and porphyrin Pd in ethanol with a concentration of $1.5 \cdot 10^{-4}$ $mol \cdot L^{-1}$ for each dye is prepared. Following the standard preparation the film is kept in the solution over night. The cells are measured and give the results reported in Table 4-5.

Table 4-5. Cell results for 1:1 mixture of black dye and porphyrin Pd under 100 mW/cm² illumination (measured at 530 nm).

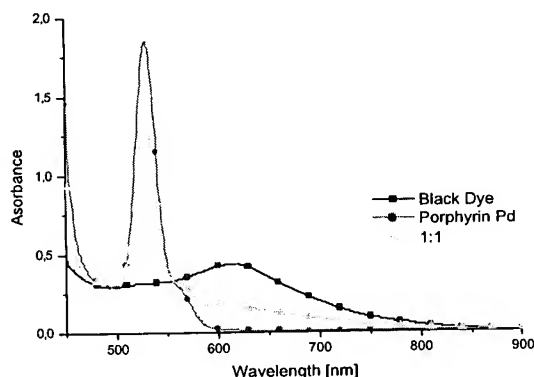|	J_{sc} [mA/cm²]	V_{oc} [mV]	FF [%]	Efficiency [%]
Cell1	13.1	580	60	4.52
Cell2	12.3	565	58	4.01
Cell3	13.4	565	57	4.42
Average	12.9	570	58	4.32
black dye	14.8	575	54	4.60
porphyrin Pd	10.7	555	68	4.03

Figure 4-8. Spectra of coloured films with black dye, porphyrin Pd and a 1:1 mixture

Also for this mixture the short circuit current density decreases linearly, this can be seen in Figure 4-9. For the efficiency the values change less and the efficiency is nearly constant.
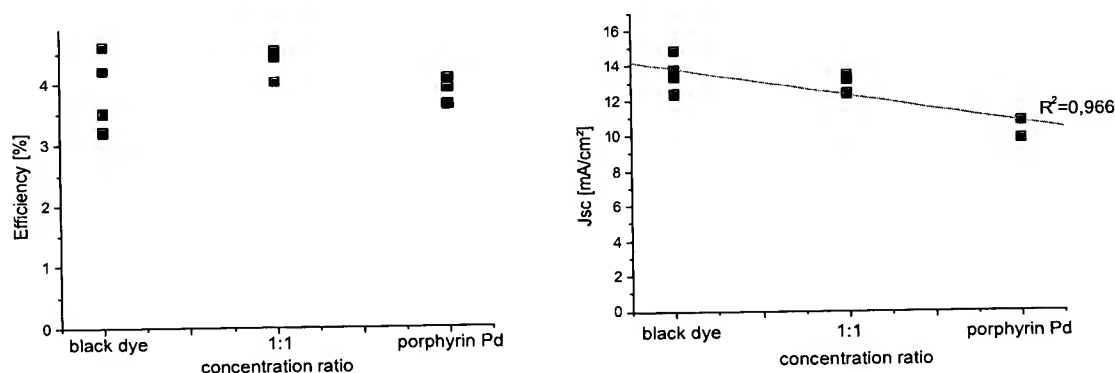

Figure 4-9. Plot of efficiency (left) and short circuit current density (right) versus the concentration ratio. The linear decrease of the current density with increasing porphyrin Pd concentration can be seen.

This experiment shows that in principle it is possible to combine two dyes with different spectra to get a mixture that can be used in a solar cell. In this case the efficiency of the mixture cell is directly in between the efficiencies of the cells with the pure dyes. To get an improved performance by means of a dye mixture, solar cells made of the single dye should give comparable results. However in this experiment no significant synergy could be detected. Maybe the 1:1 mixture is not the best ratio, but as the solar cells still do not reach the performance of

red dye bis-TBA, it seems as if it is not possible with the available dyes (red dye bis-TBA, black dye and porphyrins) to get a mixture or combination where the solar cell results are at least as high as for red dye bis-TBA. If one would have a new dye that shows a performance like red dye bis-TBA and has a spectrum clearly shifted to higher wavelength it would be worth trying such a combination, but mixtures where only one dye gives good results seem to be not useful, when operating under white light.

4.1.4 Determination of dye concentrations for mixtures

In any adsorption study the determination of the adsorbed amount of species in equilibrium with the solution is of major importance, especially for mixtures. In this particular case, one way to determine the amount of dye adsorbed at the TiO_2 surface, is by desorption experiments. With 5 mL sodium hydroxide solution ($c=1.0$ mol·L^{-1}) the dye is flushed into a 10 mL volumetric flask and filled with distilled water. From this solution UV-Vis-spectra are collected. From solutions of pure dyes in aqueous sodium hydroxide solution ($c=0.5$ mol·L^{-1}) a calibration curve can be made, from which it is now possible to determine the concentration for the pure dyes. For the mixtures the determination of concentrations is no longer possible with a simple calibration, since the spectra do overlap. For this case the multivariate data analysis provides a good tool. Spectra of dye mixtures in ethanol with known concentrations are collected. However one has to keep in mind that there is a difference in the spectra in the different solvents, the absorption maximum is shifted to shorter wavelength in basic solution compared to ethanolic solution. As this effect can be seen for both, black dye and red dye, it is to some degree acceptable to use these different solvents for the calibration and desorption solution. From the spectra a model is calculated with principle component analysis (PCA), using the Unscrambler® from CAMO Inc. (details about multivariate data analysis can be found in the appendix). For this model the complete spectrum from 400 to 900 nm is used. For the samples the desorption experiment is done and the UV-Vis spectra of the desorbed mixed dye solutions are processed with the PCA-model, with which the concentration is determined.

From the PCA-calculation, concentrations of the dyes in solution are obtained since the desorption is done quantitatively and the amount of adsorbed dye can easily be calculated. The result is a plot of amount of dye adsorbed, versus the composition of the adsorption solutions.
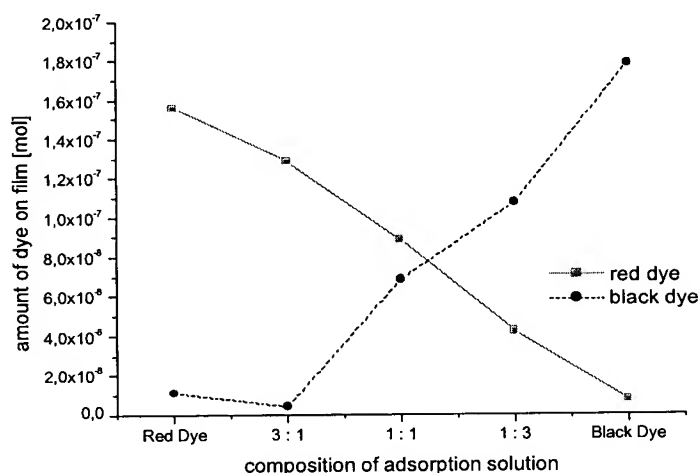
Figure 4-10. Amount of dye on a TiO$_2$ porous layer when a dye mixture with total concentration of 3.0·10^{-4} mol·L^{-1} is adsorbed over night to a titanium dioxide layer. Values calculated with PCA.

Except the mixture 3:1, for both, the red dye bis-TBA and also for black dye, there is a linear behaviour of concentration on the porous layer of TiO$_2$ and in the adsorption solution. This means in the reported mixed adsorption experiment the concentration ratio found at the interface represents the one of the dye molecules in the solution. A desired mixed concentration ratio at an interface can be adjusted by adsorbing from solutions with the corresponding ratio.

4.1.5 Adsorption experiments

Recently, possible modes of dye anchoring to a TiO$_2$ surface have been tested by molecular modelling[xii]. But a thorough characterisation of the adsorption process and sites of the sensitiser on anatase titanium dioxide, as in real photovoltaic cells at the atomic level, is still to be accomplished[xiii]. Such experiments are of crucial importance for the elucidation of the electron-transfer mechanism in these systems.

In order to get further information about the dye adsorption behaviour onto the titanium dioxide, which is important when dye mixtures are to be improved, adsorption experiments have been performed.

4.1.5.1 Isotherms

Solutions in ethanol of different concentrations are prepared for red dye bis-TBA, black dye and porphyrin Pd. Porous layers of TiO$_2$ are coloured as described before. UV-Vis-spectra are

collected from the coloured porous layers of TiO_2. As in any measurement of absorption spectra of porous layers described in this work, a clean (not coloured) porous TiO_2 layer is used as baseline. The absorption is plotted against the concentration of the solution in equilibrium. As a high excess of dye solution is used the concentration can be taken as constant, and therefore the initial concentration is used. The resulting data points can be fitted with an equation of the Langmuir type, see Equation 4-1.

$$A = A_{max} \cdot \frac{k \cdot c_{eq}}{1 + k \cdot c_{eq}}$$

A : absorption
A_{max} : plateau value of the adsorption isotherm
c_{eq} : dye molecule concentration in the solution
k : equilibrium constant for the adsorption process

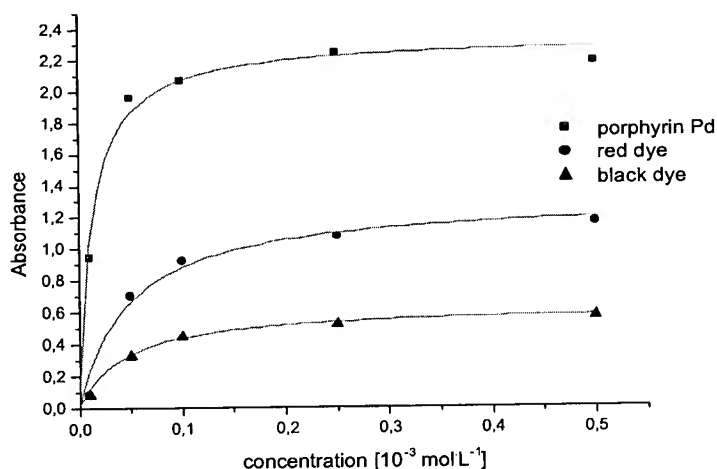**Equation 4-1. Langmuir type function used for fittings.**

Figure 4-11. Isotherms of red dye bis-TBA, black dye and porphyrin Pd at 22°C. Solid lines: Langmuir Fit to the data respectively.

Table 4-6. Values obtained at the Langmuir fit for the three dyes.

Dye	A_{max}	k
red dye bis-TBA	1.30 ± 0.10	20 ± 6
black dye	0.62 ± 0.02	22 ± 3
porphyrin Pd	2.33 ± 0.07	77 ± 13

For all three dyes the fit is possible. Above a certain dye concentration in solution the adsorption of the dye molecules saturates. However, for most systems analysed in this way, the assumptions implicit in the thermodynamic of the Langmuir model are not realised, therefore the identification of the constants obtained from the fit with physical adsorption parameters must be carefully considered. It will be assumed that the plateau value of the adsorption curves for the dyes corresponds to the surface saturation with the adsorbed species, without forming any hypothesis about the layer order of the adsorption. At a concentration of $3.0 \cdot 10^{-4}$ $mol \cdot L^{-1}$, which is generally used when preparing solar cells, the plateau is almost reached. An even higher concentration would be better, but due to solubility problems a concentration of $3.0 \cdot 10^{-4}$ $mol \cdot L^{-1}$ gives more reproducible results.

4.1.5.2 Coverage

For a quantitative comparison of the dye adsorption, the coverage θ (number of molecules per surface area) of the titanium dioxide surface with the different dye molecules is determined. Films are coloured using a standard dye solution in ethanol of a concentration of $3.0 \cdot 10^{-4}$ $mol \cdot L^{-1}$. After the films are dyed completely the dye is desorbed as described in the desorption experiment (see chapter 4.4.5). The coverage is calculated through the concentration that can be determined with a calibration curve. To get a precise concentration the calibration is made with dye solutions in 0.5 $mol \cdot L^{-1}$ aqueous sodium hydroxide to have the same conditions as in the desorption experiment and to avoid a shift in the absorption spectrum, correlated to different pH-values. The mass of the films is measured and the specific surface area of 80 m^2/g has been determined by means of BET technique. Once the coverage is known, the area per molecule (S) can be calculated. The equation that has been used is $S = \dfrac{1}{\theta_{sat}}$. The calculated values can be seen in Table 4-7.

Table 4-7. Coverage and correlating absorption of porous layers with dye, determined with desorption experiment. A_{sat}: absorbance of a porous layer of TiO_2 where the dye is adsorbed from a $3.0 \cdot 10^{-4}$ $mol \cdot L^{-1}$ solution, θ_{sat}: coverage determined in this experiment, S: area per molecule

Dye	Absorbance of film A_{sat} (λ_{max})	Coverage θ_{sat} [1/m²]	Area / molecule S [nm²]
red dye bis-TBA	0.910 (537 nm)	$7.81 \cdot 10^{17}$	1.28
black dye	0.435 (614 nm)	$6.90 \cdot 10^{17}$	1.45
porphyrin Pd	1.852 (530 nm)	$4.12 \cdot 10^{17}$	2.43

From this experiments, porphyrin Pd seems to require about twice the space as red dye bis-TBA. Assuming that porphyrin Pd attaches flat to the surface whereas red dye attaches perpendicular with two carboxylic acid groups as described by Finnie[xiv] et al. these values can be understood. Black dye needs slightly more space than red dye bis-TBA. The value that can be found in the literature[xv] for red dye of 1.65 nm² is in accordance with the value determined here. The assumption that porphyrin Pd attaches flat to the surface and therefore needs twice as much space as black dye has to be proven, if porphyrin Pd attaches even with all four carboxylic acid groups IR-spectroscopy measurements as described by Finnie et al. would be a possible measurement.

The kinetics of adsorption has been determined for black dye and porphyrin Pd. The adsorption rate is determined by measuring the change in absorption of a dye at a porous layer of TiO_2 with time. Standard porous layers of TiO_2 are prepared, and coloured in a $3.0 \cdot 10^{-4}$ mol·L^{-1} solution. Every 30 minutes the porous layers of TiO_2 are removed from the solution, and rinsed in ethanol. The absorption of the porous layers is measured and the samples are put back into the solution. The coverage is calculated through the absorption at the wavelength of maximum absorption, using Equation 4-2.

$$\theta = \frac{A_{measured[\lambda max]}}{A_{sat[\lambda max]}} \cdot \theta_{sat}$$

$A_{measured[\lambda max]}$: absorbance of porous layer at the absorption maximum

$A_{sat[\lambda max]}$: absorbance of a standard film at the absorption maximum

θ_{sat} : coverage of a standard film

Equation 4-2. Determination of the coverage θ of a porous layer of TiO_2 with a dye through the measurement of the absorption. $A_{sat[\lambda max]}$ and θ_{sat} as in Table 4-8.

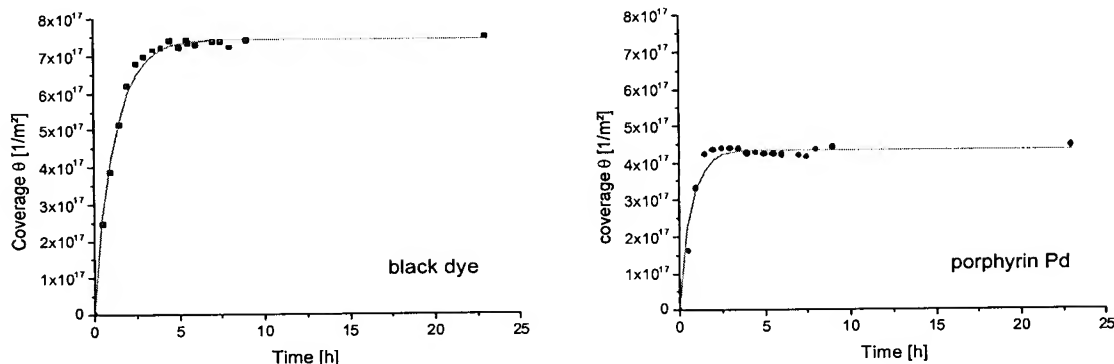The results are plotted in Figure 4-12.

Figure 4-12. Determination of the adsorption rate for black dye (left), and porphyrin Pd (right).

Many simple adsorption processes follow first order kinetics[xvi]; therefore the values are fitted with the following equation derived from a first order time law[xvii].

$$\theta = \theta_0 \left(1 - e^{-k_{ads} \cdot t}\right)$$

θ : coverage (moleculesper squaremeter)
θ_0 : maximum coverage
k_{ads} : adsorptionrate
t : time

Equation 4-3. Dependence of coverage on time.

Table 4-8. Maximum coverage and adsorption rate for black dye and porphyrin Pd.

Dye	θ_0 [1/m²]	Adsorption rate k_{ads} [h⁻¹]
black dye	$(7.43 \pm 0.05) \cdot 10^{17}$	0.83 ± 0.03
porphyrin Pd	$(4.33 \pm 0.06) \cdot 10^{17}$	1.39 ± 0.13

The adsorption rate of porphyrin Pd is 1.67 times the rate for black dye, while the coverage of black dye is 1.72 times the coverage of porphyrin Pd. Differences in the values compared with the one in Table 4-7 are due to the experimental procedures, as for example little differences in layer thickness.

In order to have more information about the strength of the chemical bond of the different dyes with TiO₂, exchange experiments have been done.

Coloured porous layers of TiO₂ with black dye or porphyrin Pd are placed into solutions of the corresponding other dye, i.e. into porphyrin Pd or black dye respectively. Again the absorption

of the porous layer is measured every 30 minutes and then they are put back into the dye solutions.
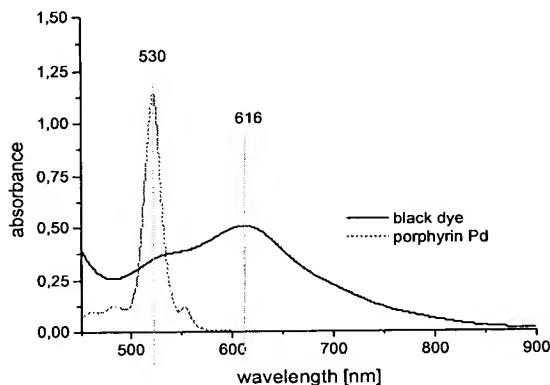

Figure 4-13. UV-Vis-Spectra of porous layers coloured with pure black dye and pure porphyrin Pd, respectively. It can be seen that at 616 nm only black dye contributes to the absorption.

Due to the difference in the absorption maximum of the two dyes, the concentration of black dye can be determined based on the absorption at 616 nm, where porphyrin Pd shows no absorption. The maximum of absorption for porphyrin Pd is at 530 nm, where also black dye absorbs. The absorption of black dye at 530 nm can be calculated with the following equation, and consequently also the absorption at 530 nm for porphyrin Pd.

$$A_{\text{black dye}[530nm]} = \frac{A_{\text{black dye standard}[530\,\text{nm}]}}{A_{\text{black dye standard}[616\,\text{nm}]}} \cdot A_{\text{measured}[616nm]}$$

$$A_{\text{porphyrinPd}[530nm]} = A_{\text{measured}[530nm]} - A_{\text{black dye}[530nm]}$$

Equation 4-4. Calculation of the absorbance at 530nm resulting from porphyrin Pd

The coverage is calculated as shown before. The determined values are plotted in Figure 4-14 and Table 4-9.
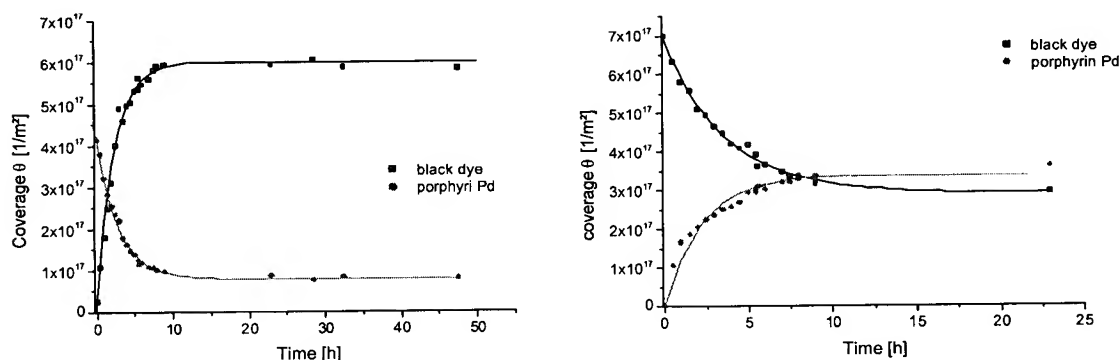
Figure 4-14. Exchange of porphyrin Pd with black dye (left), and black dye with porphyrin Pd (right). Straight lines are fitting curves.

For the description of the adsorption curve the same equation as above (Equation 4-3) has been used, while for the desorption the following equation has been applied.

$$\theta = \theta_e + A \cdot e^{-k_{des} \cdot t}$$

θ : coverage

θ_e : remaining coverage of the desorbed dye

A : amount of desorbed dye at the equilibrium $[1/m^2]$

k_{des} : desorption rate

t : time

Equation 4-5. Determination of the values for the desorption process. For derivation, see appendix.

Table 4-9. Obtained values for the exchange experiment.

Dye	θ_0 [1/m²]	θ_e [1/m²]	A [1/m²]	k_{ads} [h⁻¹]	k_{des} [h⁻¹]
porphyrin Pd	$(3.37 \pm 0.07) \cdot 10^{17}$	$(0.78 \pm 0.03) \cdot 10^{17}$	$(3.46 \pm 0.06) \cdot 10^{17}$	0.44 ± 0.03	0.35 ± 0.01
black dye	$(6.00 \pm 0.08) \cdot 10^{17}$	$(2.90 \pm 0.08) \cdot 10^{17}$	$(3.89 \pm 0.09) \cdot 10^{17}$	0.42 ± 0.02	0.28 ± 0.02

Interestingly, the exchange adsorption rate for black dye (0.42 h⁻¹) is nearly the same as for porphyrin Pd (0.44 h⁻¹). These values are much smaller than the values obtained when black dye and porphyrin Pd are adsorbed at a free TiO₂ surface (see Table 4-9). One reason for this could be that the exchange rate is just limited by the desorption process. Indeed, the desorption rates are of the same order of magnitude but still even a little bit lower, what points towards a somewhat more complicated mechanism.

A detailed look at the saturation values shows that if porphyrin Pd is replaced by black dye, the amount of black dye that adsorbs is about 1.7 times the amount of porphyrin Pd that dissolves. In the other case, if black dye is replaced by porphyrin Pd, the amount of porphyrin Pd that adsorbs is nearly the same as black dye that dissolves. In accordance with the previous discussion, the first result can be understood in terms that porphyrin Pd needs twice the space than black dye, as at each place where porphyrin Pd is dissolved up to two molecules black dye can adsorb. For the reverse process it seems that on each place where one black dye dissolves one molecule porphyrin Pd can add, which points towards a different adsorption geometry of the porphyrin Pd, i.e. not flat on the surface.

With our methods it cannot be shown why porphyrin Pd needs about twice the space as red dye or black dye.

One very likely possibility, as already mention, is that porphyrin Pd attaches flat to the surface with up to four carboxylic acid groups, whereas red dye and black dye attach perpendicular with only two acid groups. Another possibility is that both attach perpendicular or tilted to the surface with up to two acid groups, where porphyrin Pd needs more space due to its potentially bigger system of delocalised π-electrons.

Another interesting point is why a saturation of the dye that is first adsorbed can be observed, and what is the reason that it does not desorb completely. One possible explanation is that there exist two possibilities of dye adsorption (discussed here for red dye)[xviii]: the first one with the dye attached with only one carboxylic acid group; molecules attached in this way dissolve more easily as they are dissolved as soon as the sole bond is released. The second one is with the dye attached also with the second carboxylic acid group. This state is very stable as the dye is still attached if one bond is released, and as the desorption occurs on a long timescale this bond can be reformed before also the second bond is released and the whole molecule is dissolved. However, this theory has to be proven with further experiments or measurements, but in the literature[xix] similar explanations can be found.

4.2 Increasing the dye concentration at the surface

Besides the extension of the effective absorption range of the adsorbed dye molecules in the visible part of the spectrum, another way to enhance the efficiency of the solar cell is to increase the dye concentration at the surface.

When the red dye bis-TBA adsorption is performed in the presence of silver ions in the dye solution the photovoltaic performance of solid-state dye-sensitised solar cells can be improved significantly[xx]. The explanation, given by Krüger et al., is that two dye molecules form dimers via the isothiocyanate ligands, and therefore more dye is adsorbed to the surface, which is proven with a higher dye concentration at the surface. We found an even higher increase in efficiency when the dye adsorption is performed in the presence of cobalt, in this case the complexation occurs via the carboxylic acid groups of the ligands. One difficulty however is the fact that the silver and cobalt ions have to be removed from the cell by rinsing with an iodide solution. Otherwise they would react with the iodide in the electrolyte and precipitate, which could lead to a change of the titanium dioxide dye / electrolyte interface in a negative way.

Table 4-10. Comparison of cells where dye is adsorbed with and without the presence of silver and cobalt ions.

Modification	J_{sc} [mA/cm²]	V_{oc} [mV]	FF [%]	Efficiency [%]
standard	21.3	630	60	8.08
Dye with Ag^+	19.9	650	55	7.12
Dye with Ag^+, Ag^+ washed out	19.8	725	64	9.20
Dye with Co^{2+}	20.5	615	60	7.54
Dye with Co^{2+}, Co^{2+} washed out	19.4	720	68	9.52

A more convenient way to enhance the concentration of the dye molecules without having the problem of removing the Ag^+ or Co^{2+} ions would be to bridge two molecules via chemical bonds.

From the results above it can be seen that a complexation via the acid groups gives the best results, therefore a chemical modification towards a Ru-complex dimer via the carboxylic acid groups of the ligands seems most promising. Such a chemical modification, where two dye molecules are bridged via the carboxylic acid groups using alkyl chains by means of an amide or an ester bond, would possibly not change the electronic properties of the dye significantly.

Furthermore the presence of hydrophobic chains can afford an improvement in the stability of solar cell performances, emerging from the water insolubility of these dyes. Moreover it can be possible to use weak forces (van der Waals contacts and hydrogen bonds) to induce a higher degree of order at the TiO_2 surface.

At a first glance the modification of the preformed dye seemed to be easier, but after a few trials, the modification of the bipyridine ligand and subsequent synthesis of a new dye was much more straightforward. As a test system, non-functionalised alkyl chains are attached to a dye molecule. The next step further is the synthesis of chemically bonded dimer via the bipyridine ligand.

4.2.1 Modification of Ru-complex

The amidation of two carboxylic acid groups of the red dye is tried, using the carbodiimide coupling with an excess of red dye. The reaction scheme is shown in Figure 4-15.
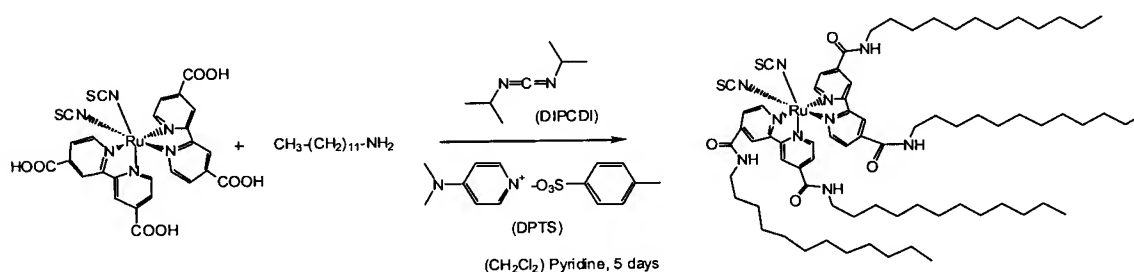
Figure 4-15. Reaction scheme for the carbodiimide coupling of red dye with an amine.

25 mg ($3.54 \cdot 10^{-5}$ mol) red dye, 13.8 mg ($7.44 \cdot 10^{-5}$ mol) dodecylamine and 43.8 mg ($1.49 \cdot 10^{-4}$ mol) 4-N,N-dimehtylaminopyridinium 4-toluenesulfonate (DPTS) are given into a dry 25 mL flask. 7 mL dry pyridine is added, and the mixture is dissolved while heating. The mixture is cooled down to room temperature and 18.76 mg ($1.49 \cdot 10^{-4}$ mol) diisopropyl carbodiimide (DIPCDI) is added. The mixture is stirred at room temperature for 5 days. The solvent is evaporated and the solid is dried under vacuum. The product is purified with column chromatography packed with aluminium oxide and tetrahydrofuran (THF) as eluent. The separated red solid obtained is dissolved in diethyl ether to isolated from the insoluble diisopropyl urea (yield 7.7 mg, 20%).

The product is characterised by UV-Vis, ^{1}H-and ^{13}C-NMR-spectroscopy, see appendix.
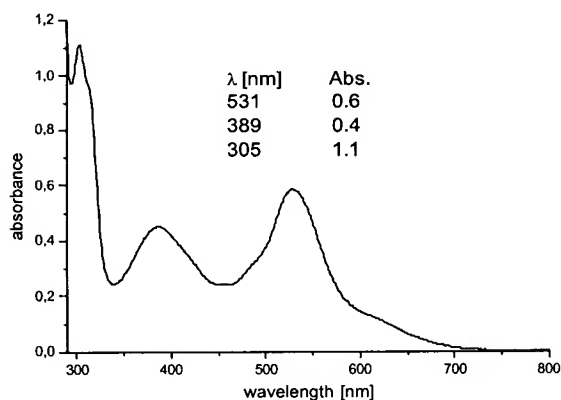
Figure 4-16. UV-Vis spectrum of the modified dye.

Even though red dye was used in excess, the product received is a fully substituted complex where no free carboxylic acid group is left. Therefore, this complex has no possibility to be attached to the TiO$_2$ surface, and cannot be used to sensitise titanium dioxide.

In order to overcome this problem, the ligands have to be modified first and then used to build the desired complex.

4.2.2 Modification of the ligand

There are two strategies to synthesise the modified red dye with the characteristics wanted. In one case an asymmetric bipyridine ligand can be used to build up a symmetric complex, in the other case two symmetric ligands can be used to build up an asymmetric complex. The two paths are shown in the scheme below.
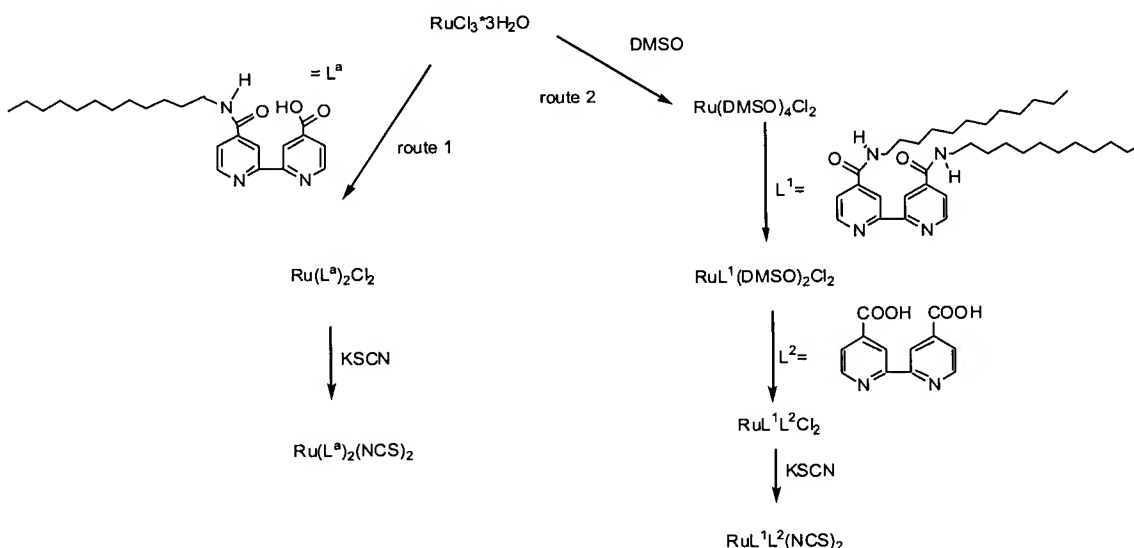
Figure 4-17. Scheme of the two ways to modify the ligands.

In both cases, the first step is the synthesis of the ligands, or better the modification of the bipyridine dicarboxylic acid, e.g. to form an amide.

Using an excess of bipyridine dicarboxylic acid, in order to realise a statistical reaction towards di -and monoamide, it was not possible to isolate the asymmetric bipyridine ligand, i.e. the monoamide (route1, Figure 4-17). Therefore the strategy followed is to synthesise asymmetric dye molecules, starting from the $Ru(DMSO)_4Cl_2$, and attaching successively the modified ligand and the bipyridine dicarboxylic acid according to route 2, Figure 4-17.

In particular, the following asymmetric Ru-complexes are synthesised (see Figure 4-18).
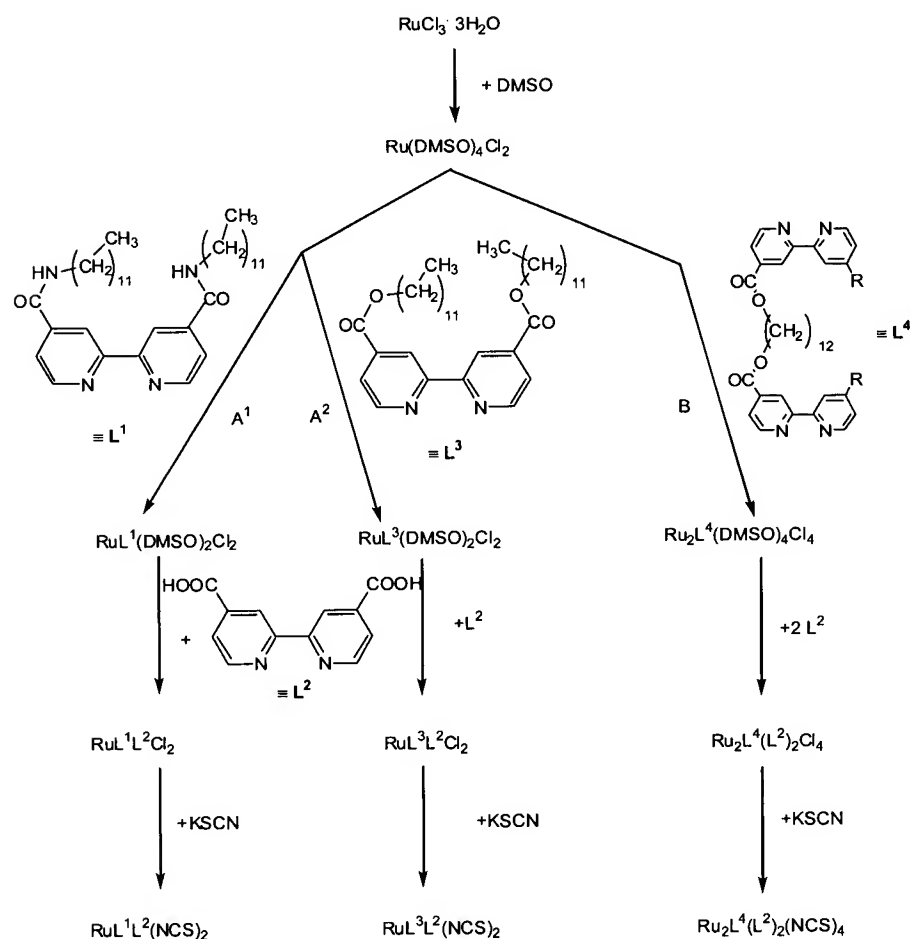
Figure 4-18. Schematic reaction route for Ru-complex.

Two isomers of the Ru-complexes are possible regarding the isothiocyanate ligans. Due to the electronic and steric properties the cis-configuration is favoured, which has to be considered at the synthesis.
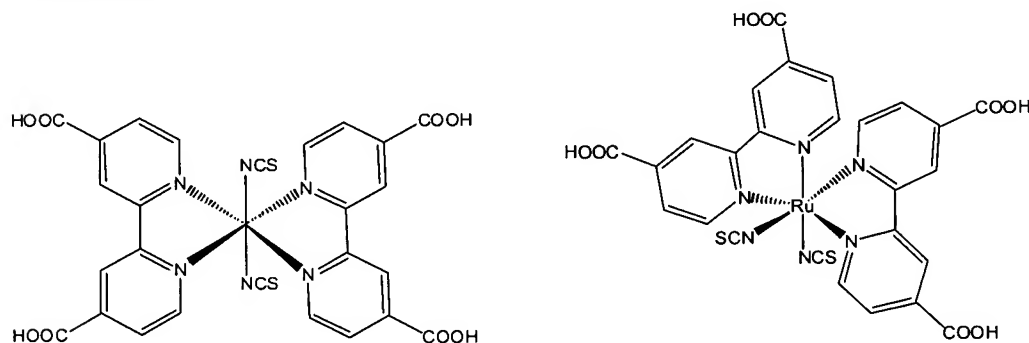
Figure 4-19. Two isomers of the Ru-complex, trans-configuration (left), and desired cis-configuration (right).

4.2.3   Synthesis of the symmetric ligands

4.2.3.1   Synthesis of N,N'-Didocecyl-2,2'bipyridine-4,4'dicarboxamide (L^1)

600 mg bipyridine dicarboxylic adic (L^2) (2.46·10^{-3} mol) are weighed into a 50 mL flask, and 6 mL thionylchloride (SOCl$_2$) are added. The mixture is heated up to 76 °C and refluxed for 3 hours. After letting cool down to room temperature the product precipitates. The excess of SOCl$_2$ is distilled according to the literature[xxi], and the product dried under vacuum for 2 hours. Without further purification the acid chloride is dissolved in 10 mL dry toluene, and 600 mg dodecylamine (3.69·10^{-3} mol) are added. The mixture is heated to 110 °C, and refluxed for 2 hours.
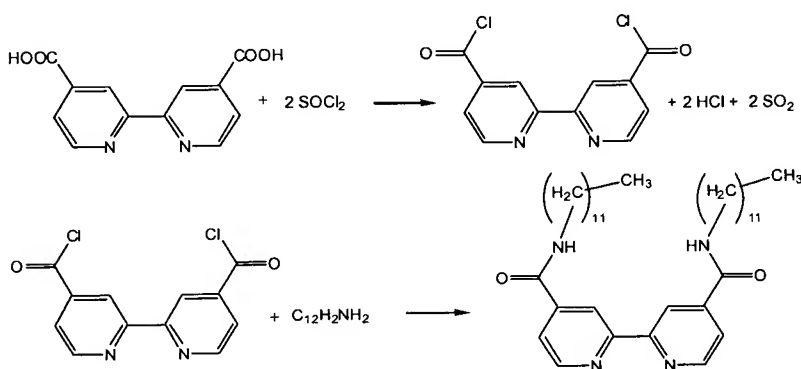
Figure 4-20. Reaction of N,N'-Didocecyl-2,2'bipyridine-4,4'dicarboxamide, L^1

After letting cool down to room temperature the mixture is treated with cold sodium hydrogen carbonate solution and chloroform is added. At the interface a solid precipitated. The organic phase and the precipitate are separated. Chloroform is evaporated, and the crude product purified by column chromatography using aluminium oxide, and a mixture of THF and methanol 1:2 as eluent. The second fraction obtained, is the same as the solid that precipitated in the separation funnel. The product is identified by IR and ^{1}H-NMR-spectroscopy as the disubstituted product (yield 1.1 g, 83 %).
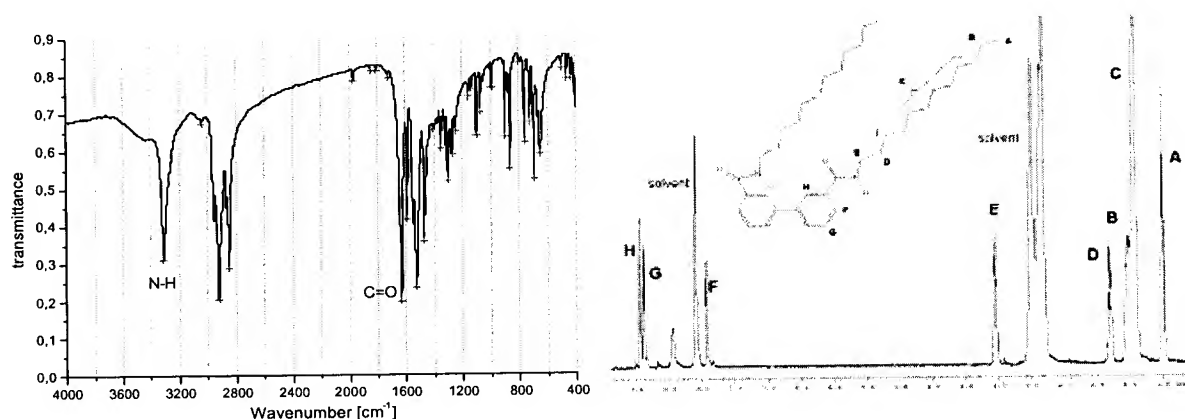
Figure 4-21. FT-IR spectrum and ¹H-NMR of modified ligand L¹. The IR spectrum is measured in KBr. The ¹H-NMR spectrum is measured in DMF-d7 at 120°C.

In the IR-spectrum the N-H-stretching of the secondary amide at 3313 cm⁻¹, and the C=O-stretching at 1633 cm⁻¹ are clearly visible, but no broad O-H-stretching of a free carboxylic acid group between 3200 and 2500 cm⁻¹.

The ligand L¹ is hardly soluble in any solvent when precipitated once, which might be due to very strong hydrogen bonds among the amide-groups. Therefore the same reaction is done with dodecanol to form the ester, which is easier to dissolve for the further processing.

4.2.3.2 Synthesis of Didodecyl-2,2'-bipyridine-4,4'-docarboxylate (L³)

1 g (4.1·10⁻³ mol) L² and 10 mL SOCl₂ are refluxed for 4 hours. The excess of SOCl₂ is distilled, and the solid dried under vacuum for 2 hours. 450 mg (1.6·10⁻³ mol) of the product and an excess of dodecanol, 800 mg (4.3e-3 mol), are dissolved in 10 mL dry toluene, and refluxed for 2 hours. After letting cool down to room temperature the mixture is treated with cold sodium hydrogen carbonate solution, and chloroform is added. The organic phase is dried over magnesium sulphate, filtered, the solvent is evaporated, and a yellow product is isolated. This crude product is purified by column chromatography using silica gel and THF as eluent. The yellow colour is removed but there is still unreacted dodecanol. The alcohol can be removed by recrystallisation from a chloroform / acetone mixture (yield 2.12 g, 89 %).
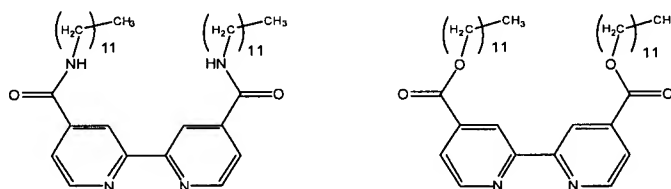
Figure 4-22. Structures of the modified ligands. Amide (L^1) (left), ester (L^3) (right).

4.2.4   Building the Ru-complex with the amide L^1

The first step is the synthesis of the tetra-DMSO ruthenium dichloride[xxii] $(Ru(DMSO)_4Cl_2)$ starting with ruthenium trichloride trihydrate. Then one ligand is introduced after the other.

4.2.4.1   Synthesis of Dichlorotetrakis(dimethyl sulfoxide)ruthenium(II) (Ru(DMSO)$_4$Cl$_2$)

300 mg ($1.15 \cdot 10^{-3}$ mol) Ruthenium trichloride trihydrate ($RuCl_3 \cdot 3H_2O$) are dissolved in 3 mL dimethyl sulphoxide and refluxed for 5 minutes. The colour turns from dark brown to orange.
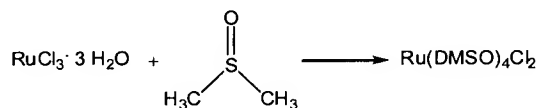
Figure 4-23. Forming Ru(DMSO)$_4$Cl$_2$ the first step to the modified Ru-complex.

The volume is reduced and acetone is added to precipitate the product, which is filtered and dried under vacuum. No further purification was required. The product is characterised by ^{1}H-NMR-spectroscopy (yield 401 mg, 72 %).

4.2.4.2   Synthesis of Dichloro(N,N'-didodecyl-2,2'-bipyridine-4,4'-dicarboxamide)bis-(dimethyl sulfoxide)-ruthenium (II) (RuL^1(DMSO)$_2$Cl$_2$)

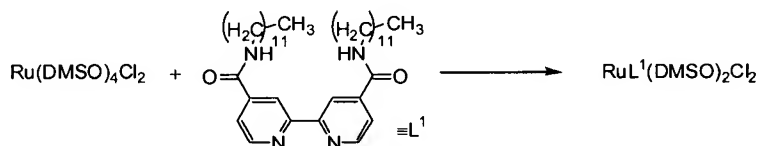**Figure 4-24. Introduction of the first ligand to the Ru-complex**

200 mg ($4.13 \cdot 10^{-4}$ mol) Ru(DMSO)$_4$Cl$_2$ are dissolved in chloroform, and 238 mg ($4.13 \cdot 10^{-3}$ mol) L^1 are added. The mixture is refluxed for 1.5 hours under nitrogen. After letting cool down to room temperature, the mixture is filtered, the solvent evaporated, and the solid then redissolved

in acetone. The unreacted Ru(DMSO)$_4$Cl$_2$, which is not soluble in acetone, is removed by filtration. After reducing the volume, the complex is precipitated with petrol ether (yield 197 mg, 53 %).

4.2.4.3 Synthesis of cis-Dichloro(N,N'-didodecyl-2,2'-bipyridine-4,4'-dicarboxamide)(2,2'-bipyridyl-4,4'-dicarboxylato)-ruthenium(II) (RuL^{1}L^{2}Cl$_2$)

110 mg (1.21·10^{-4} mol) RuL^1(DMSO)$_2$Cl$_2$ are dissolved in 50 mL DMF, and 30 mg (1.21·10^{-4} mol) bipyridin dicarboxylic acid (L^2) are added. The mixture is refluxed under nitrogen for 4 hours in darkness, to avoid cis-trans-isomerisation. After letting cool down, the mixture is filtered. The solvent is evaporated and the remaining solid dissolved in methanol and filtered again. The volume is reduced, and the product precipitated with petrol ether. The product is filtered and dried.
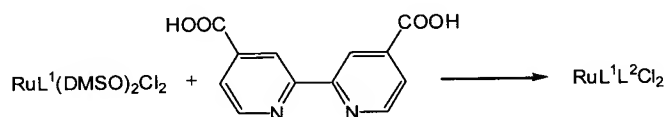

Figure 4-25. Introduction of the second ligand to the Ru-complex

4.2.4.4 Synthesis of cis-bis(isothiocyanato)(N,N'-didodecyl-2,2'-bipyridine-4,4'-dicarboxamide) (2,2'-bipyridyl-4,4'-dicarboxylato)-ruthenium (II) (RuL^{1}L^2(NCS)$_2$)

370 mg (3.8·10^{-3} mol) potassium thiocyanate are dissolved in 3 mL water and transferred into a three-necked flask. 50 mL DMF are added, and the solution is purged with nitrogen for 5 minutes. 100 mg (1.0·10^{-4} mol) RuL^{1}L^{2}Cl$_2$ are added and the whole mixture is refluxed for 5 hours in the dark. The solution is cooled down and filtered. The solvents, DMF and water, are evaporated. The viscous product is dissolved in chloroform, and water is added to extract the water-soluble potassium thiocyanate. The red coloured organic phase is separated, and the solvent is evaporated. The product is purified with column chromatography using Sephadex LH-20 as stationary phase and methanol as eluent. No sharp bands could be detected and therefore three fractions have been collected.
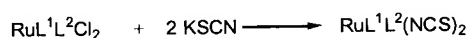

Figure 4-26. Substitution of Cl-ions by NCS-ions.

4.2.4.5 Synthesis of cis-bis(isothiocyanato)(Didodecyl-2,2'-bipyridine-4,4'-dicarboxylate) (2,2'-bipyridyl-4,4'-dicarboxylato)-ruthenium (II) (RuL³L²(NCS)₂)

148 mg ($3.05\,10^{-4}$ mol) Ru(DMSO)₄Cl₂ and 177 mg ($3.05\,10^{-4}$ mol) L³ are dissolved in 25 mL chloroform and refluxed for 1.5 hours. Then the solvent is evaporated and the solid purified using column chromatography with silica gel and THF. 65 mg ($7.15\,10^{-5}$ mol) of the dried product RuL³(DMSO)₂Cl₂ and 17 mg ($7.15\,10^{-5}$ mol) L² are dissolved in 25 mL DMF, and refluxed for 4 hours. The solvent is evaporated and the remaining solid redissolved in methanol. The solution is filtered, the volume reduced and the product precipitated with petrol ether. In a three-necked flask 230 mg ($7.5\,10^{-5}$ mol) potassium thiocyanat are dissolved in 1.5 mL water, and 10 mL DMF are added. The dried precipitate is added, and the whole mixture is refluxed for 5 hours in darkness. After cooling down, the solution is filtered and the solvents are evaporated. The remaining viscous red liquid is dissolved in chloroform, and water is added to extract the excess of potassium thiocyanate. The organic phase is evaporated, and the product separated with column chromatography using Sephadex LH-20 as stationary phase and methanol as eluent. Also here three fractions have been colected.

Table 4-11. Overview of obtained fractions.

	Modified dye as amide RuL¹L²(NCS)₂	Modified dye as ester RuL³L²(NCS)₂
1st Fraction	RuL¹L²(NCS)₂-1	RuL³L²(NCS)₂-1
2nd Fraction	RuL¹L²(NCS)₂-2	RuL³L²(NCS)₂-2
3rd Fraction	RuL¹L²(NCS)₂-3	RuL³L²(NCS)₂-3

As it is not clear in which fraction the desired product is and even with ¹H-NMR spectra an answer cannot be found, all fractions are dissolved in ethanol and UV-Vis-spectra are collected.
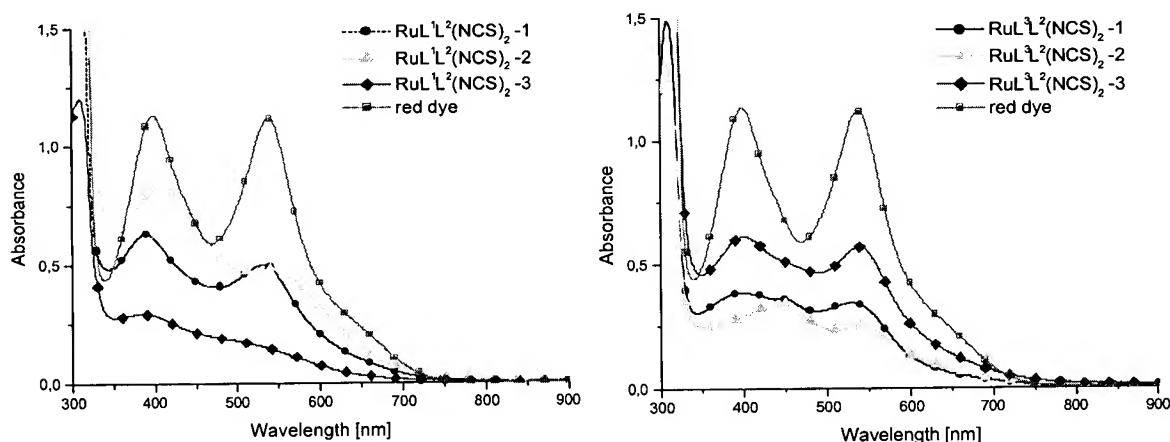
Figure 4-27. UV-Vis-spectra of ethanolic solution of all six fractions. Left: amide-modified, right: ester-modified.

From the UV-Vis-spectra it can be seen that all the fractions have two absorption maxima in the range between 350 and 700 nm. In the case of fraction 2 of the dye modified as ester a third absorption maximum at 452 nm can be detected and can be associated to an impurity. In any case it is not easy to decide where the desire product is.

An empirical method is used to see if the separated complexes have bipyridine dicarboxylic acid ligands. FTO-substrates are coated with porous layers of TiO_2 of K65 and KTP (a new paste that gives more transparent porous layers of TiO_2, which is better for collecting UV-Vis-spectra) and placed into the different solutions of fraction of the ester modified dye $(RuL^3L^2(NCS)_2)$. Then the absorption of the substrates and the solution is measured.

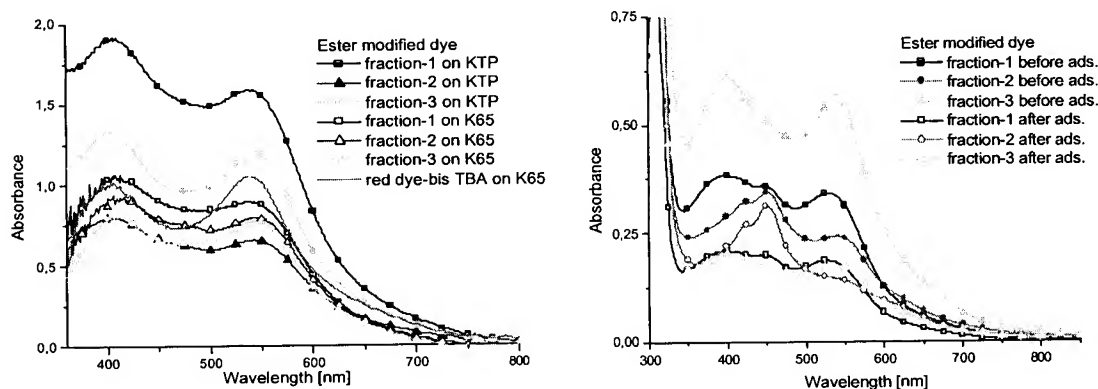**Figure 4-28. Spectra of coloured films of K65 and KTP with different fractions of the ester modified dye $RuL^3L^2(NCS)_2$ (left). Spectra of the solutions before and after the adsorption (right).**

All the absorption spectra obtained from the different fractions and with the different porous layers are similar:

They all have two maxima, near 410 nm, and 550 nm. It seems that from all dye solutions the same complex adsorbs at the titanium dioxide surface. At the same time, some of the remaining dye solutions changed the relative intensities of the absorption peaks before and after the adsorption drastically. For example, the absorption at 460 nm, which was attributed to an impurity, increases relative to the two maxima at 410 nm and 550 nm. Furthermore the solution turned browner.

This is a hint that the desired complex can be found in each fraction, with more or less impurities. The adsorption-experiment shows that only the complex adsorbs to TiO_2 and the impurities remain in the solution.

Out of those six dye solutions, solar cells are prepared. Porous layers of TiO_2 are prepared with K65, and placed into the mentioned solutions.

As the dye concentration in the adsorption solution is unknown, spectra of the solutions are collected and the absorption values are compared to get the relative concentration.
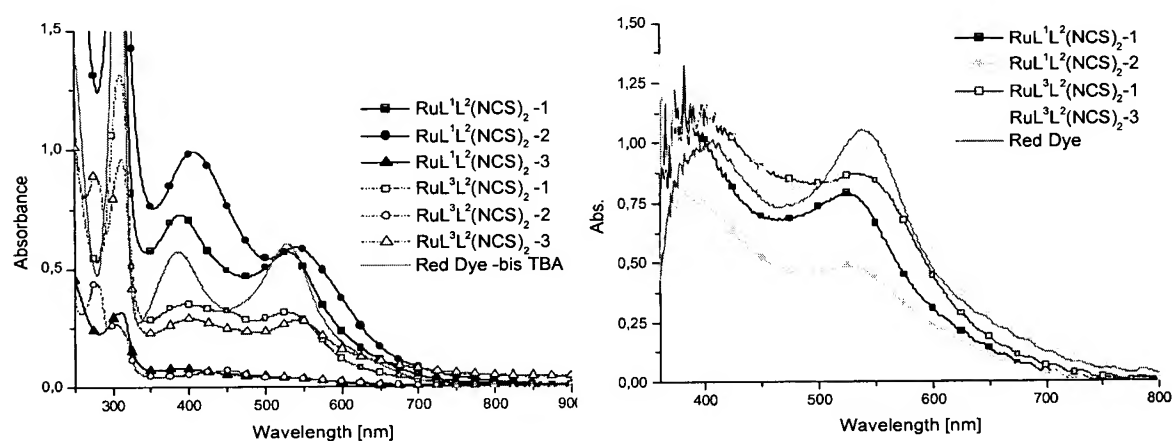

Figure 4-29. Spectra of solution used for dye adsorption for solar cells (left). Spectra of coloured films for solar cells (right).

The two solutions, $RuL^1L^2(NCS)_2$-3 and $RuL^3L^2(NCS)_2$-2, that show a very low absorption and did not colour the substrates properly were not used for solar cells. The remaining four solutions and one reference solution of red dye bis-TBA are used to prepare cells. UV-Vis-spectra of the coloured porous layers are collected before adding the electrolyte, to enable a qualitative comparison of the adsorbed dye molecules, comparing the absorption peak between 530 and 550

nm. The intensity of the absorption peak of the first fraction of the amide-modified dye complex is slightly lower than of the first fraction of the ester-modified complex, and slightly shifted to lower wavelength, which might have its origin in the amide functionality. The absorption maximum of the second fraction of the amide-modified complex is much lower than of the other fractions. Finally the absorption of the third fraction of the ester-modified dye complex is comparable to red dye bis-TBA and slightly higher than the corresponding first fraction.

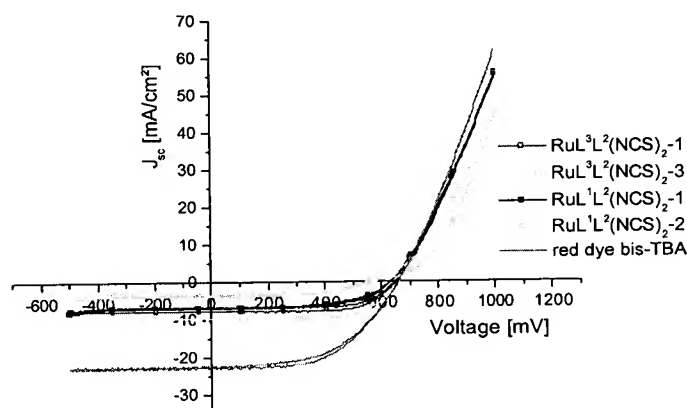The ready solar cells are measured and the following results are obtained.

Figure 4-30. Results of solar cells made of the modified dye, measured at 100 mW/cm²

Table 4-12. Results of solar cells made of the modified dye and one reference cell made of red dye bis-TBA, at 100 mW/cm² light intensity (measured at 530 nm).

	J_{sc} [mA/cm²]	V_{oc} [mV]	Fill Factor [%]	Efficiency [%]
red dye bis-TBA	23.10	660	54	8.24
$RuL^3L^2(NCS)_2$-1	7.85	650	70	3.56
$RuL^3L^2(NCS)_2$-3	9.72	660	70	4.46
$RuL^1L^2(NCS)_2$-1	6.71	630	64	2.70
$RuL^1L^2(NCS)_2$-2	3.80	575	56	1.22

The solar cells made with the third fraction of the ester-modified dye complex, $RuL^3L^2(NCS)_2$-3, show with an efficiency of 4.46 % the best results among the solar cells based on the modified dye. However the reference cell, with red dye bis-TBA, has an efficiency more than twice as high, with a significantly higher current density. One reason for the difference in the results might be the different concentrations of adsorbed dye at the porous TiO_2 layer. However,

according to the UV-Vis results, this was not expected to result in such a big difference. Probably the alkyl chains changed the wetting behaviour of the electrolyte and therefore the recombination of the dye molecules at the TiO_2 interface. Furthermore, even so the esterification of the red dye should not change the electronic nature of the molecule so much, it might be that that the charge injection is more difficult.

4.3 Equipment

4.3.1 Spray pyrolysis

The blocking layer is applied by spraying with a Merck TLC sprayer.

4.3.2 Screen printing

Screen-printing is made using a commercial screen printer, with custom-made screens of different mesh sizes and patternings. The mesh size describes the number of wires per inch, and determines the resulting layer thickness. The substrate is fixed by vacuum. The titanium dioxide paste is printed on the substrate through a screen with mesh size 30 which results, after the sinter process, in the following porous TiO_2 layers thicknesses:

paste K40: 5.8 μm   paste K65: 6.9 μm   paste KTP: 8.4 μm

4.3.3 Hot Plate

For sintering the porous layer, and for the blocking layer preparation a hot plate with programmable temperature unit is used.

4.3.4 UV-Vis spectrometer

Collecting UV-Vis-spectra is done with a Varian Cary 50 spectrometer.

4.3.5 Solar cell characterisation

The I-V-characteristic of the solar cells is measured in darkness and under illumination, using a Keithley Source-Measure Unit 236 SMU that is PC-controlled using a LabView program. This program also calculates the values for J_{sc}, V_{oc}, FF and η.

4.3.6 Light source for solar cell characterisation

The standard light source is a sulphur lamp from IKL Celsius and Fusion Lightning INC: Sulphur-lamp Light Drive 1000^{TM}, type 1400 – E2/1.
The Light intensities are measured with a Coherent Fieldmaster. Standard light intensity: 100 mW/cm^2 measured at 530 nm.

4.3.7 NMR Spectrometer

NMR spectra are measured with a 400 MHz Bruker NMR.

4.3.8   IR-Spectrometer

Infrared spectra are collected with a Bruker IFS 66/S spectrometer.

4.3.9   Glove Box

The glove box used is a UniLab from M.Braun.

4.4   Recipes and Operations

In this diploma thesis all work is done according to the following recipes and operations, if not mentioned different.

4.4.1   Cleaning of fluorine doped tin oxide (FTO) coated glass

Substrates are cleaned by treating 15 minutes in the ultrasonic bath with each of the following solutions: acetone, 2 % of volume aqueous Hellmanex, millipore water and iso-propanol. After acetone the substrates are rinsed with water, after Hellmanex they are rinsed 10 times with water. The cleaned substrates are stored in iso-propanol.

4.4.2   Blocking Layer

The blocking layer is prepared as follows: The substrates are heated on the hotplate to 450 °C, an ethanolic solution of titanium acetylacetonate (0.2 $mol\cdot L^{-1}$) is sprayed with a TLC sprayer onto the substrates. Each cycle consists of 2 passes and should take approximately 4 seconds; the cycles are applied in 1-minute intervals. After the 4th cycle, the substrates are heated up to 500 °C, kept there for 60 minutes and then cooled down to room temperature. The program for the blocking layer is: heating in 20 minutes to 450°C, stay for 15 minutes, heating in 5 minutes to 500°C, stay for 60 minutes, cool down to room temperature.

4.4.3   Porous Layer of TiO_2

The porous layer is prepared by screen-printing technique. Special highly viscous pastes are use, consisting of TiO_2-nanoparticles and organic filling material. All the solar cells prepared in the frame of this thesis are based on paste K65. For UV-Vis spectroscopy experiments paste K40 was used. Possible bubbles formed in the wet porous layer are removed by blowing slightly over it.

The substrates with the wet porous layer are placed onto the hotplate and sintered. The program for the porous layer is: heating in 20 minutes to 80°C, rest for 30 minutes, heating in 20 minutes to 450°C, rest for 30 minutes, cool down to 80°C.

After letting cool down to 80 °C the substrates are dipped into the dye solution and kept there for 16 h. After 16 h the substrates are removed from the dye solution, rinsed with ethanol and dried with nitrogen.

4.4.4 Dye solution

The dye solution is prepared by weighing the equivalent mass of $15 \cdot 10^{-6}$ mol into a 50 mL volumetric flask, mixing it with some absolute ethanol, and keeping for 15 minutes in the ultrasonic bath at room temperature. The flask it filled up to the mark with absolute Ethanol, resulting in a $3 \cdot 10^{-4}$ mol·L^{-1} solution. This solution is kept in the darkness until used.

Table 4-13. Mass of the dyes used to preparea a 310^{-4} mol·L^{-1} solution. 1) batch number 020701T, 2) batch number 220601T

Dye	Molar mass [g·mol^{-1}]	Mass for 50 mL solution [mg]
red dye bis-TBA[1]	1188.6	17.9
black dye[2]	640.6	9.6
porphyrin H$_2$	790.8	11.8
porphyrin Co	847.7	12.7
porphyrin Cu	852.3	12.8
porphyrin Pd	895.2	13.5
porphyrin Pt	983.8	14.8
porphyrin Zn	854.2	12.8

4.4.5 Electrolyte and backelectrode

The electrolyte is prepared in the glove box to prevent diffusion of water and oxygen.

The coloured and dried porous layer substrates are filled with electrolyte and sandwiched with the Pt-counter-electrode. Thereby on two opposite sides, small parts of polycarbonate spacer film are placed with a thickness of 6 μm. They function as spacer between the working and the counter electrode. To measure over a defined solar cell area a mask with a hole of defined area is placed onto the transparent working electrode. The whole 'sandwich' is kept together with clamps.

4.4.6 Cell Measurement

The IV-characteristic of the solar cells is first measured in the dark, then three times while illuminating with 100 mW·cm^{-2}. The best solar cell of each series is then measured with reduced light using intensities of 80, 50, 25 and 10 mW·cm^{-2}. Illumination is done from the working electrode side (FTO-electrode)

4.4.7 Desorption experiment

The desorption experiment is done to determine the amount of dye adsorbed to a porous layer of defined volume. The porous layer is printed on a glass substrate, sintered and dyed with the desired dye.

With 5 mL of a 1 mol·L^{-1} sodium hydroxide solution the dye is flushed from the substrate into a 10 mL volumetric flask, which is then filled with distilled water to the mark. From these solutions UV-Vis-spectra are collected to determine the concentration using a previously made calibration plot of absorbance versus concentration.

5 Bibliography

[i] Grätzel, M., *Nature* **414**, 338-344 (2001).

[ii] Halme, J., Dye-sensitised nanoporous and organic photovoltaic cells: technical review and preliminary tests, Espoo 2002.

[iii] Grätzel, M., *Prog. Photovolt. Res. Appl.* **8**, 171-185 (2000).

[iv] Kalyanasundaram, K.;Grätzel, M., *Coordination Chemistry Reviews* **177**, 347-414 (1998).

[v] Park et al., *J. Phys. Chem. B* **104**, 8989-8994 (2000).

[vi] Matthews et al., *Solar Energy Materials & Solar Cells* **44**, 119-155 (1996).

[vii] Wolfbauer, G., The electrochemistry of dye-sensitized solar cells, their sensitizers and their redox-shuttles, Melbourne July 1999.

[viii] "Number of dyes synthesized for solar cell applications." S. Jenkins, **1998**.

[ix] G. Smestad, C. Bignozzi and R. Argazzi, *Sol. Energy Mater. Sol. Cells* **32(3)**, 259-272 (1994).

[x] H. Tsubomura, M. Matsumura, Y. Nomura and T. Amamiya, *Nature* **261**, 402-403 (1976).

[xi] Tsuda et al, *J. Am. Chem. Soc.* **123**, 10304-10321 (2001) and references 1-3 therein.

[xii] Shklover, V.; Ovchinnikov, Yu. E.; Braginsky, L. S.; Zakeeruddin, S. M; Grätzel, M., *Chem. Mater.* **10**, 2533 (1998).

[xiii] Zubavichus et al., *Chem. Mater.* **14**, 3556-3563 (2002).

[xiv] Finnie et al., *Langmuir* **14**, 2744, (1998).

[xv] Hagfeldt and Grätzel, *Acc. Chem. Res.* **33**, 269-277(2000).

[xvi] Andrew Zangwill, Physics at surfaces, Cambridge University Press, 1988.

[xvii] Peter W. Atkins, Physikalische Chemie 1. Auflage, VCH Verlagsgesellschaft mbH Weinheim, 1987, S.710.

[xviii] Fillinger et al., *J. Electrochem. Soc.* **149**, A1146-A1156 (2002).

[xix] Fillinger et al., *J. Electrochem. Soc.* **146**, 4559-4564, (1999).

[xx] Krüger et al., *Appl. Phys. Lett.* **81**, 367 (2002).

[xxi] Sprintschnik et al., *Journal of the American Chemical Society* **99**, 4947 (1977).

[xxii] Evans, I.P.; J.C.S. Dalton 1972.

6 Appendix

6.1 Multivariate data analysis

Principal Components Analysis: Basic Ideas

The Alchemist at http://www.chemweb.com   31 March 2000

PCA is probably the most widespread multivariate statistical technique, and because of the importance of multivariate measurements in chemometrics, it is regarded by many as the technique that most significantly changed the chemist's view of data analysis, writes Richard Brereton.

History

There are numerous claims to the first use of PCA in the literature. Probably the most famous early paper was by Pearson in 1901 [1]. However, the fundamental ideas are based on approaches well known to physicists and mathematicians for much longer, namely those of eigenvector analysis. In fact, some school mathematics syllabuses teach ideas about matrices which are relevant to modern chemistry. An early description of the method in physics was by Cauchy in 1829 [2]. It has been claimed that the earliest non-specific reference to PCA in the chemical literature is 1878 [3], although the author of the paper almost certainly did not realise the potential, and was dealing mainly with a simple problem of linear calibration.

It is generally accepted that the revolution in the use of multivariate methods took place in psychometrics in the 1930s and 1940s of which Hotelling's paper is regarded as a classic [4]. An excellent recent review of the area with a historical perspective, available in the chemical literature, has been published by the Emeritus Professor of Psychology from the University of Washington, Paul Horst [5].

Psychometrics is well understood to most students of psychology and one important area involves relating answers in tests to underlying factors, for example, verbal and numerical ability as illustrated in Figure 1. PCA relates a data matrix consisting of these answers to a number of psychological "factors". In certain areas of statistics, ideas of factor analysis and PCA are intertwined, but in chemistry both approaches have a different meaning.
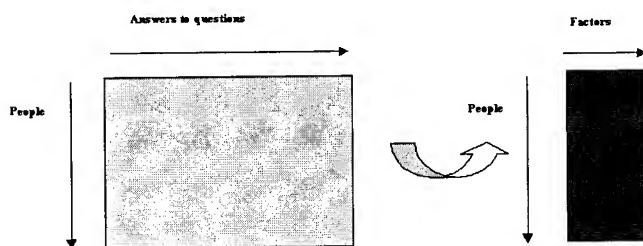

Figure 31

Natural scientists of all disciplines — biologists, geologists and chemists — have caught on to these approaches over the past few decades. Within the chemical community the first major applications of PCA were reported in the 1970s, and form the foundation of many modern chemometric methods.

Multivariate data matrices

A key idea is that most chemical measurements are inherently *multivariate*. This means that more than one measurement can be made on a single sample. An obvious example is spectroscopy: we can record a spectrum at hundreds of wavelength on a single sample. Conventional approaches are *univariate* in which only one wavelength (or measurement) is used per sample, but this misses much information. Another common area is quantitative structure property activity relationships, in which many physical measurements are available on a number of candidate compounds (bond lengths, dipole moments, bond angles etc.), can we predict, *statistically*, the biological activity of a compound? Can this assist in pharmaceutical drug development? There are several pieces of information available. PCA is one of several multivariate methods that allows us to explore patterns in this data, similar to exploring patterns in psychometric data. Which compounds behave similarly? Which people belong to a similar group? How can this behaviour be predicted from available information?
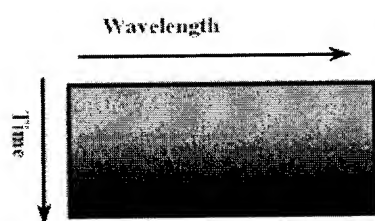
Figure 32
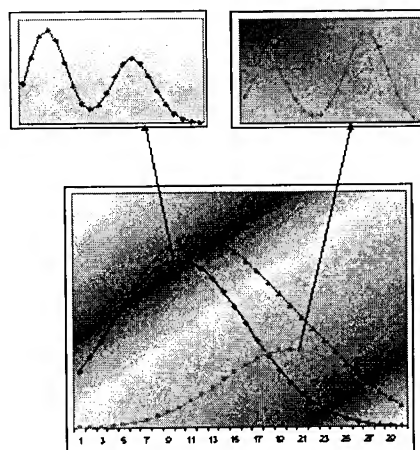
Figure 33

As an example, Figure 2 represents a chromatogram in which a number of compounds are detected with different elution times, at the same time as at their spectra (such as a uv of mass spectrum) are recorded. Coupled chromatography, such as diode array high performance chromatography or liquid chromatography mass spectrometry, is increasingly common in modern laboratories, and represents a rich source of multivariate data. The chromatogram can be regarded as a data matrix.

What do we want to find out about the data? How many compounds are in the chromatogram would be useful information. Partially overlapping peaks and minor impurities are the bug-bears of modern chromatography. What are the spectra of these compounds? Figure 3 (*above*) represents some embedded peaks. Can we reliably determine these spectra? Finally, what are the quantities of each component? Some of this information could undoubtedly be obtained by better chromatography, but there is a limit, especially with modern trends to recording more and more data, more and more rapidly. And in many cases the identities and amounts of unknowns may not be available in advance. PCA is one tool from multivariate statistics that can help sort out these data.

Aims of PCA

The aims of PCA are to determine underlying information from multivariate raw data.

There are two principle needs in chemistry. In the case of the example from coupled chromatography we would like to extract information from the two-way chromatogram.

The number of significant PCs is ideally equal to the number of significant components. If there are three components in the mixture, then we expect that there are only three PCs.

Each PC is characterised by two pieces of information, the *scores*, which, in the case of chromatography, relate to the elution profiles and the *loadings*, which relate to the spectra.

In the next article we will look in more detail how this information is obtained. However, the ultimate information has a physical meaning to chemists.

The second need is simply to obtain patterns. Figure 4 represents the result of performing PCA on a series of chromatographic measurements on a number of different compounds using eight different commercial columns. The dimensions of the data matrix are chromatographic columns and results of various tests (e.g. elution times, peak widths and peak asymmetries), rather than elution times and spectra or people and answers to psychological tests. The aim is to show which columns behave is a similar fashion. The picture suggests that the three Inertsil columns behave very similarly whereas Kromasil C-18 and Supelco ABZ+ behave in a diametrically different manner. This could be important, for example, in the determination of which columns are best for separating basic compounds, which for amino acids and which for neutral compounds. The resultant picture is a principal component plot, and later articles will outline a number of different ways of obtaining and interpreting such pictures.
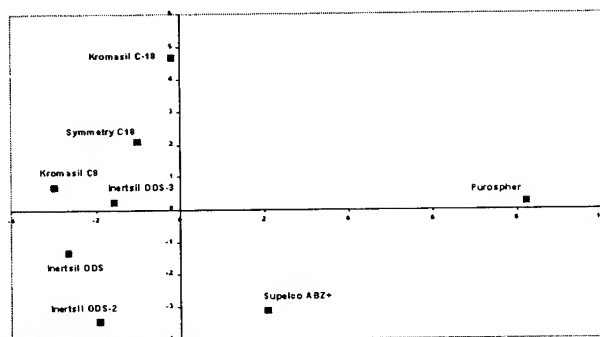

Figure 34

PCA has a fundamental and important role in many areas of chemometrics. Later articles will concentrate on different aspects in detail.

References

1. Pearson K (1901). **On lines and planes of closest fit to systems of points in space.** *Phil. Mag.* 6:(2) 559–572.

2. Cauchy A.L (1829), Oeuvres, IX (2), 172–175

3. Adcock, R.J. (1878) A problem in least squares, The Analyst, 5, 53–54

4. Hotelling. H. (1933). **Analysis of a complex of statistical variables into principal components.** *J. Educ. Psychol.*, 24, 417–441, 498–520

5. Horst P. (1992). **Sixty years with latent variables and still more to come**, *Chemometrics and Intelligent Laboratory Systems*, 14, 5–21.

Principal Components Analysis: a Second Look

Previously we discussed the origins of PCA in chemistry; now we will look at the main ideas behind PCA. Although chemists have developed their own terminology, it is essential to recognise that similar principles occur throughout scientific data analysis, whether in physics, quantum mechanics or psychology, writes Richard Brereton.

Chemical Factors

As an illustration, we will use the case of coupled chromatography, such as diode array HPLC. For a simple chromatogram, the underlying dataset can be described as a sum of responses for each significant compound in the data, which are characterised by (a) an elution profile and (b) a spectrum, plus noise or instrumental error. In matrix terms, this can be written as

$$X = C \cdot S + E$$

where

X is the original data matrix or coupled chromatogram,

C is a matrix consisting of the elution profiles of each compound,

S is a matrix consisting of the spectra of each compound,

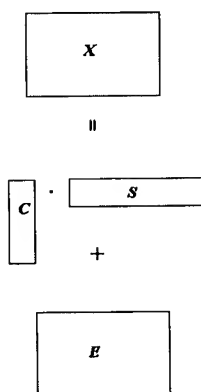E is an error matrix.

This is illustrated in Figure 5.

Figure 35

Consider a two-way chromatogram recorded over 10 minutes at 1-second intervals (600 points in time), and over 200 nm at 2 nm intervals (100 points in time), containing 3 underlying compounds.

X is a matrix of 600 rows and 100 columns,

C is a matrix of 600 rows and 3 columns, each column corresponding to the elution profile of a single compound,

S is a matrix of 3 rows and 100 columns, each row corresponding to the spectrum of a single column,

E is a matrix of the same size as X.

If we observe X, can we then predict C and S? Many chemometricians use a "hat" notation to indicate a *prediction* so it is also possible to write the equation above as

$$X \approx \hat{C}.\hat{S}$$

Ideally the predicted spectra and chromatographic elution profiles are close to the true ones, but it is important to realise that we can *never directly or perfectly* observe the underlying data. There will always be measurement error even in practical spectroscopy. Chromatographic peaks may be partially overlapping or even embedded meaning that chemometric methods will help resolve the chromatogram into individual components.

One aim of chemometrics is to obtain these predictions after first treating the chromatogram as a multivariate data matrix, and then performing PCA. Each compound in the mixture is a "chemical" factor with its associated spectra and elution profile, which can be related to principal components, or "abstract" factors, by a mathematical transformation.

Rank and eigenvalues

A fundamental first step is to determine the number of significant factors or components in a matrix. In a series of mixture spectra or portion of a chromatogram, this should, ideally, correspond to the number of compounds under observation.

The *rank* of a matrix relates to the number of significant components in the data, in chemical terms to the number of compounds in a mixture. For example, if there are 6 components in a chromatogram the rank of the data matrix from the chromatogram should ideally equal 6. However, life is never so simple. What happens is that noise distorts this ideal picture, so even though there may be only 6 compounds, it may appear that the rank is 10 or more.

Normally the data matrix is first transformed into a number of principal components and the *size* of each component is measured. This is often called an *eigenvalue*: the earlier the components the larger their size. It is possible to express eigenvalues as a percentage of the entire data matrix, by a simple technique.

Determine the sum of squares of the entire data, S_{total},

For each principal component determine its own sum of squares (which is often equal to the sum of squares of the scores vector as discussed below), S_k for the kth component. This is a common definition the *eigenvalue* although there is other terminology in the literature.

Determine the percentage contribution of each principal component to the data matrix (100 S_k / S_{total}). Sometimes the *cummulative* contribution is calculated.

One simple way of determining the number of significant components is simply by the looking at the size of each successive eigenvalue. Table 1 illustrates this. The total sum of squares for the entire dataset is 670, so since the first three principal components account for around 95% of the data, it is a fair bet that there are only 3 components in the data. There are, of course, more elaborate approaches to estimating the number of significant components, to be discussed in later articles.

	PC1	PC2	PC3	PC4	PC5	Total sum of squares
Eigenvalue	300	230	109	20	8	670
Explained variance in %	44.78	34.38	16.27	2.99	1.19	
cumulative variance in %	44.78	79.108	95.37	98.36	99.55	

The number of significant components will never be more than the smaller of the number of rows and columns in the original data matrix X. Hence if this matrix consists of 600 rows (e.g. chromatographic elution times) and 100 columns (e.g. spectral wavelengths), there will never be more than 100 non-zero eigenvalues, but, hopefully, the true answer will be very much smaller, reflecting the number of compounds in the chromatogram.

Scores and Loadings

PCA results in an abstract mathematical transformation of the original data matrix, which, for the case of a coupled chromatogram, may take the form

$$X \approx \hat{C}.\hat{S} = T.P$$

where T are called the scores, and are the same size as C, and P the loadings and are the same size as S. A big interest is how to relate the abstract factors (scores and loadings) to the chemical factors. Note that the product and number of abstract factors should ideally equal the product and number of chemical factors. Purely numerical techniques can be use to obtain the abstract factors.

Each scores matrix consists of a series of column vectors, and each loadings matrix a series of row vectors, the number of such vectors equalling the rank of the original data matrix, so if the rank of the original data matrix is 8 and spectra are recorded at 100 wavelengths, the loadings matrix consists of 8 row vectors 100 datapoints in length. Many authors denote these vectors by t_k and p_k where k is the number of the principal component (1, 2, 3 up to the

rank). The scores matrices *T* and *P* are composed of several such vectors, one for each principal component. These can be related to the true spectra and elution profiles by a transformation as illustrated in Figure 6, where appropriate.
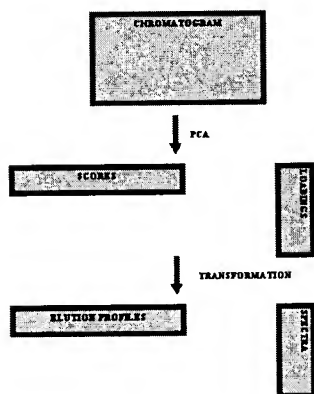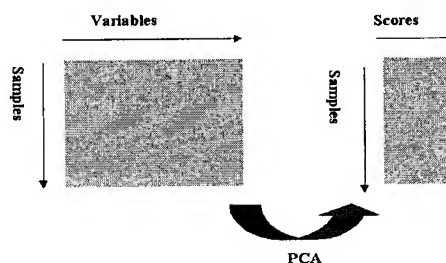

Figure 36

Figure 37

In certain areas of chemical pattern recognition, the scores and loadings are an end in themselves and no further transformation to physical factors is required.

Scores and loadings have important properties, the main one being *orthogonality*. This is often expressed in a number of ways.

The sum of the product between any two loadings or scores vectors is 0.

The correlation coefficient between any two loadings or scores vectors is 0.

The original variables (e.g. 100 wavelengths) are reduced to a number of significant principal components (e.g. 3 or 4) each of which orthogonal to each other. In practice, PCA has acted as a form of variable reduction, reducing the large original dataset (e.g. recorded at 100 wavelengths) to a much smaller more manageable dataset (e.g. consisting of 3 principal components) which can be interpreted more easily, as illustrated in Figure 7. The loadings represent the means to this end.

The loadings vectors for each component are generally normalised, meaning that their sum of squares equals one, whereas the sum of squares of the scores vectors are often equal to the corresponding eigenvalue.

14 April 2000

6.2 Derivation of equations for adsorption and exchange process

$$\begin{bmatrix} \text{dye} \end{bmatrix}_{\text{surface}} \quad \rightleftharpoons \quad \begin{bmatrix} \text{dye} \end{bmatrix}_{\text{solution}}$$

Derivation of the equation for the adsorption process:

$$\frac{d\theta}{dt} = -K \cdot c \cdot (1-\theta)$$

$$\int \frac{d\theta}{1-\theta} = -\int K \cdot c \cdot dt$$

$$\ln[1-\theta] = -Kct + C$$

$t = 0$..

$0 = C$

$$(1-\theta) = e^{-kt}$$

$$\theta = 1 - e^{-kt}$$

$t \rightarrow \infty$

$$\theta = \theta_0$$

$$\Rightarrow \quad \theta = \theta_0 \left(1 - e^{-kt} \right)$$

Derivation of the equation for the desorption process:

$$\frac{d\theta}{dt} = -k \cdot \theta$$

$$\int \frac{d\theta}{\theta} = -\int k \cdot dt$$

$$\ln[\theta] = -Kt + C$$

$t = 0$..

$$\ln \theta_a = C$$

$$\ln \theta = -kt + \ln \theta_a$$

$$\ln \theta - \ln \theta_a = -kt$$

$$\ln \frac{\theta}{\theta_a} = -kt$$

$$\frac{\theta}{\theta_a} = e^{-kt}$$

$$\Rightarrow \quad \theta = \theta_a \left(e^{-kt} \right)$$

skaling to θ :

$$\theta = \theta_e + \theta_a e^{-kt}$$

6.3 NMR-Spectra
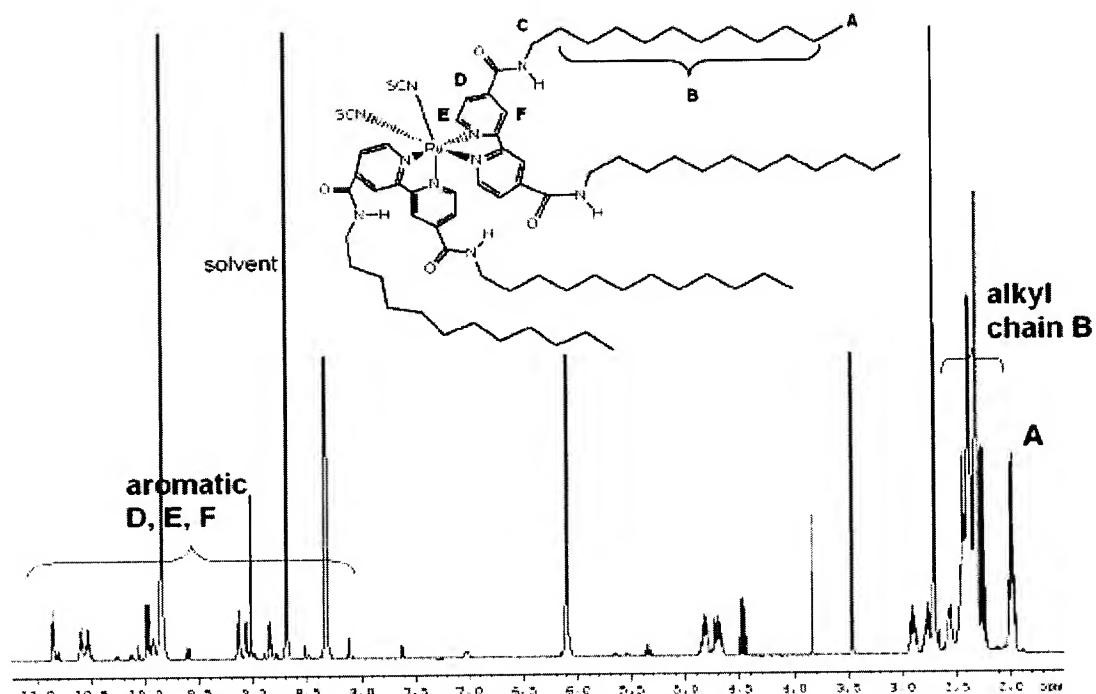
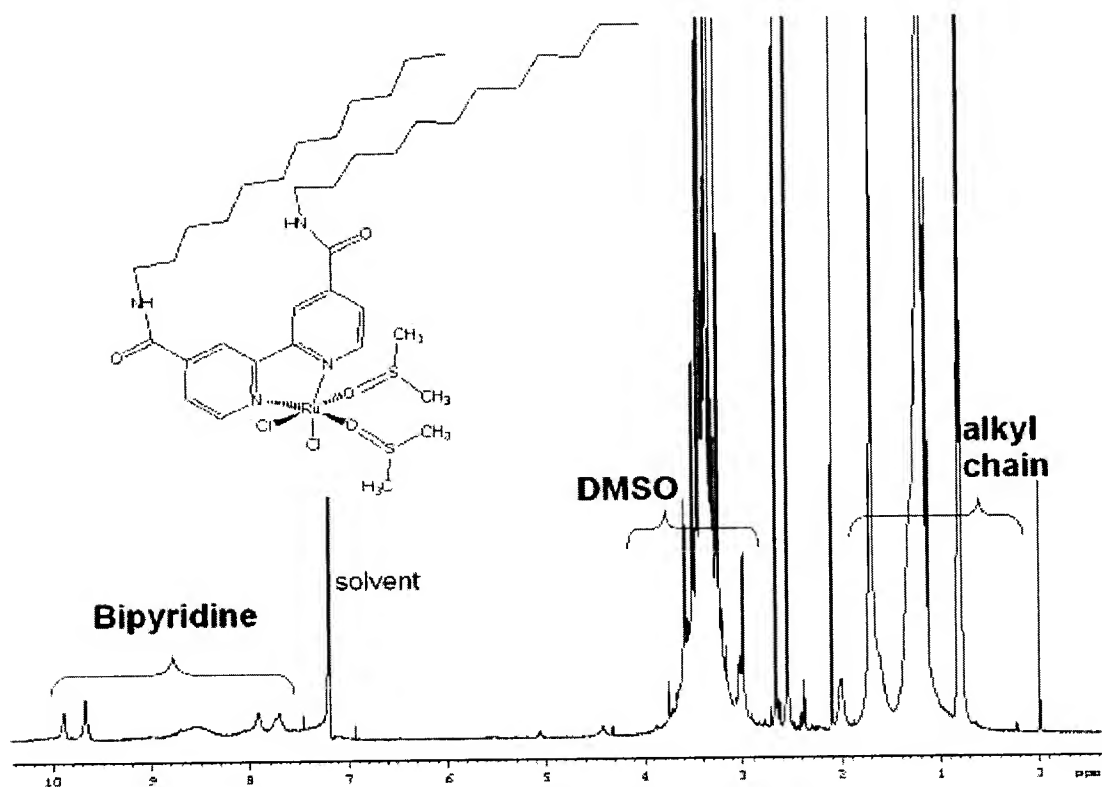^{1}H-NMR (Pyridine-d5): modified red dye, not further purified
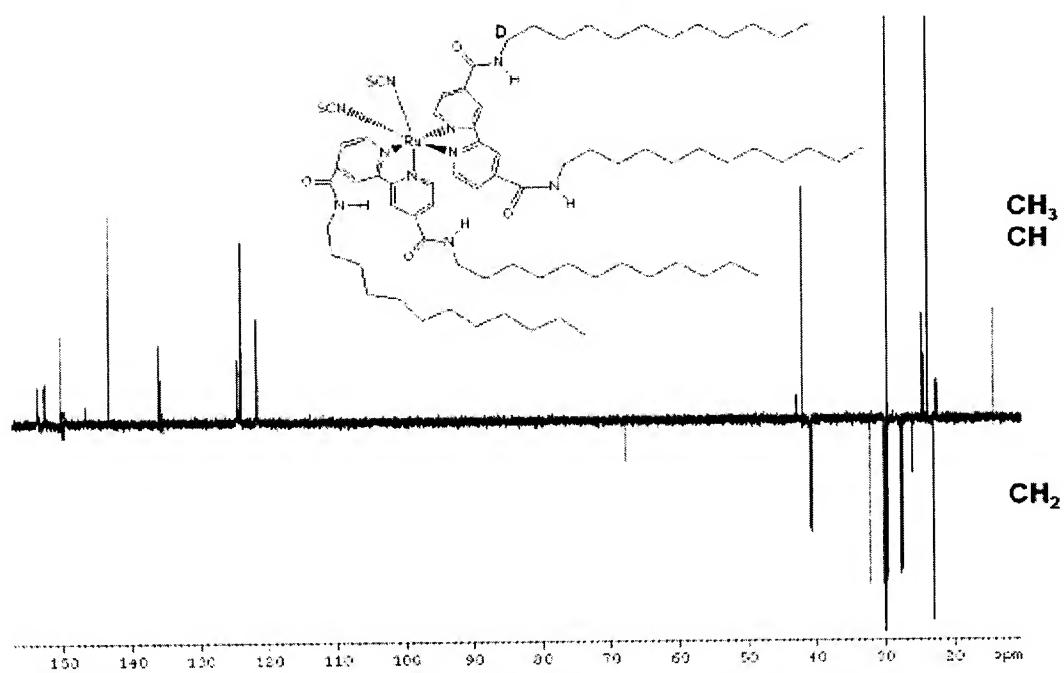
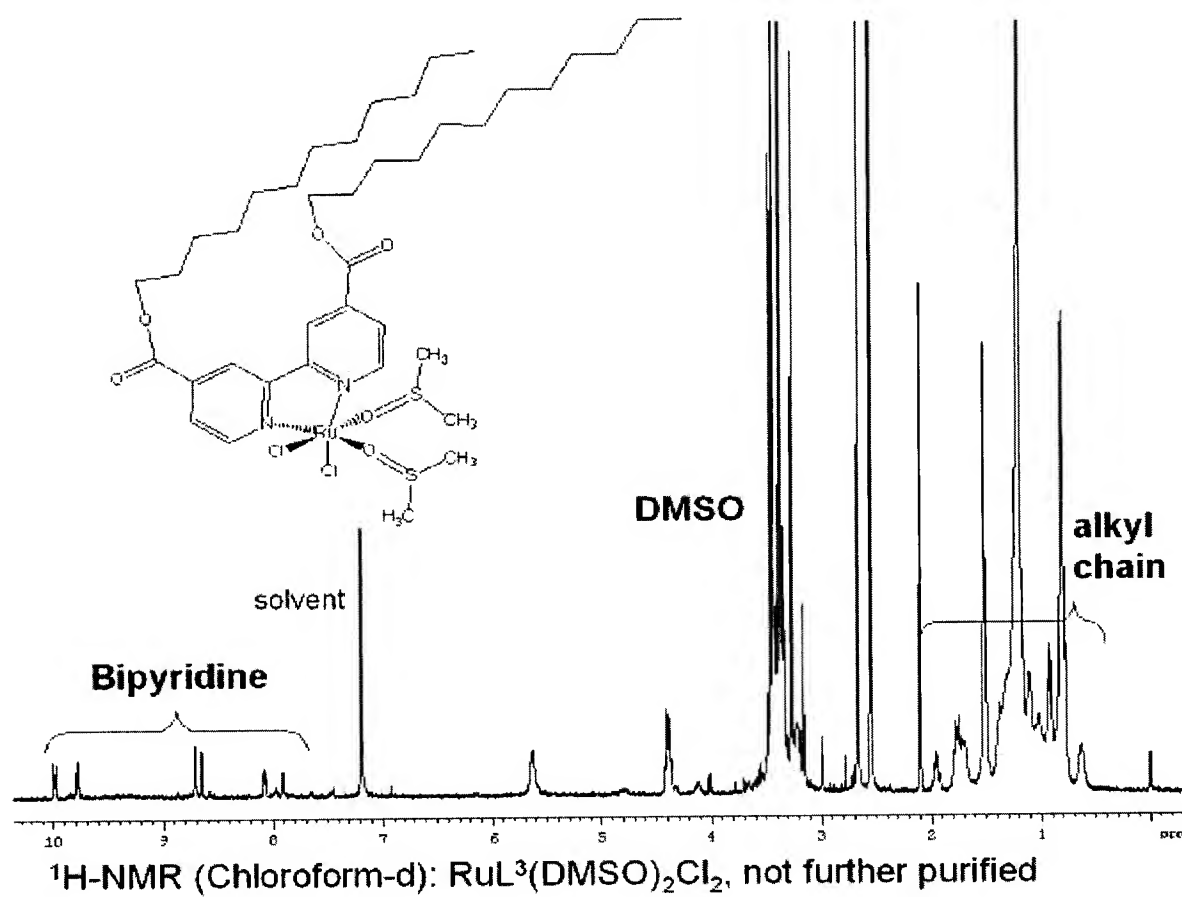^{13}C-DEPT (Pyridine-d5): modified red dye, not further purified

¹H-NMR (DMF-d7): amide modified ligand (L¹), at 120°C

¹H-NMR (Chloroform-d): ester modified ligand (L³)
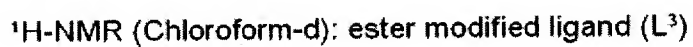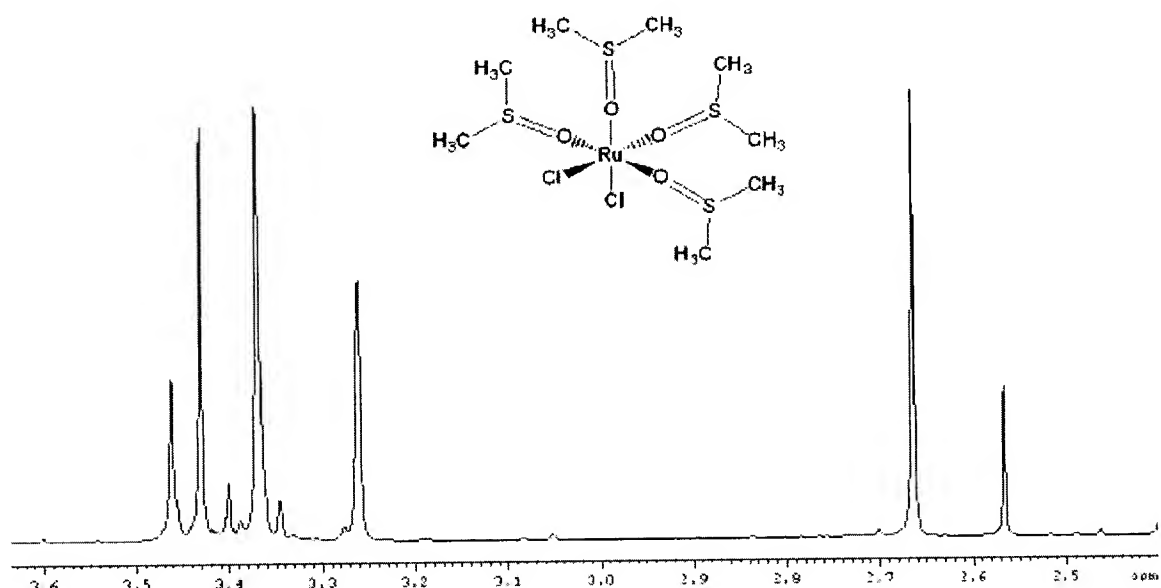
¹H-NMR (Chloroform-d): Ru(DMSO)₄Cl₂

¹H-NMR (Chloroform-d): RuL¹(DMSO)₂Cl₂, not further purified

^{1}H-NMR (Chloroform-d): RuL^3(DMSO)$_2$Cl$_2$, not further purified

Ich versichere, dass ich diese Diplomarbeit selbständig verfasst, keine anderen als die angegebenen Quellen und Hilfsmittel benutzt, sowie alle wörtlich oder sinngemäß übernommenen Stellen in der Arbeit gekennzeichnet habe. Diese Arbeit wurde noch keiner Kommission zur Prüfung vorgelegt und verletzt in keiner Weise Rechte Dritter.

_____